Coherence and the Origin of Optical Sum Rule Violations in Cuprate Superconductors

Michael Norman

Materials Science Division
Argonne National Laboratory

Catherine Pepin -SPhT
Mohit Randeria – Tata

Emery +
Kivelson

Nature '95

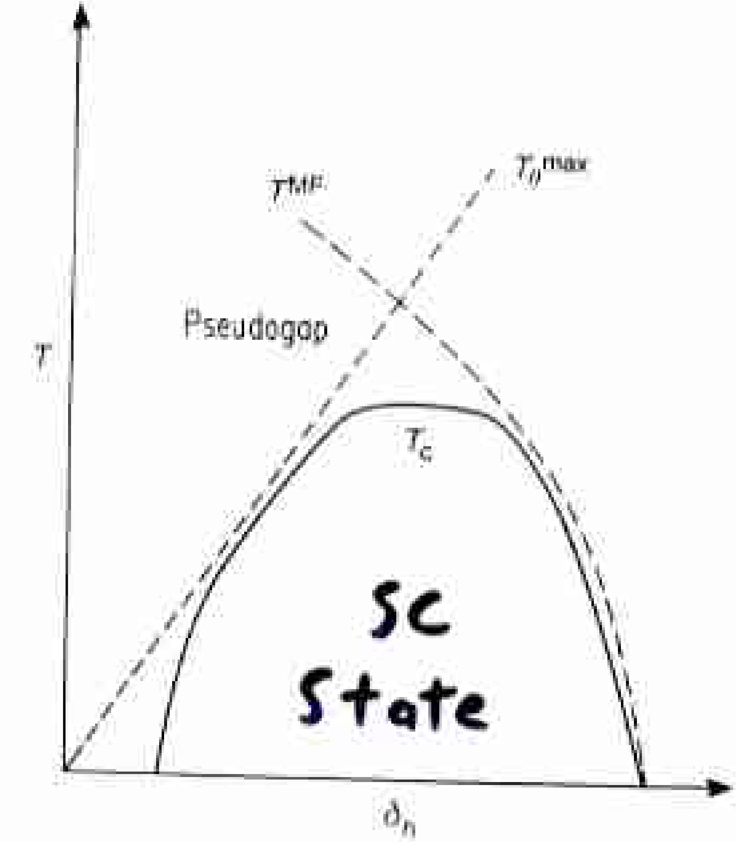

FIG. 1 A sketch of the phase diagram of high-temperature superconductors as a function of temperature T and doping δ_n. T^{MF} is the mean-field transition temperature, T_θ^{max} the upper bound on the phase ordering temperature, and T_c the actual transition temperature. The form of T^{MF} for small δ_n depends on the mechanism of superconductivity and the precise role of doped-insulator effects.

of superconductor but rather a more-or-less gradual crossover in behaviour as the value of T_θ^{max}/T_c changes. Furthermore, the values of this ratio given in Table 1 are subject to the uncertainties in the experimental values of $\lambda(0)$ and the precise form of the short-distance cutoff. But the systematic variation of the properties of high-temperature superconductors from one material to another clearly supports the importance of phase fluctuations. Our analysis suggests a new interpretation of the usual phenomenological classification of high-temperature superconductors into three, more-or-less distinct categories: 'underdoped', 'optimally doped' and 'overdoped'. The value of T_c is predominantly determined by phase fluctuations in underdoped high-temperature superconductors such as $YBa_2Cu_4O_8$ ($T_\theta^{max}/T_c \approx 1$), and by the mean-field transition temperature T^{MF} in overdoped materials such as Tl 2201 ($T_\theta^{max}/T_c \gtrsim 2$). Optimally doped materials, such as $YBa_2Cu_3O_{7-\delta}$ and $La_{2-x}Sr_xCuO_4$, with δ and x in the neighbourhood of 0.05 and 0.15, respectively, are in the crossover region between the two. (Note that the use of the a-axis value of λ for $YBa_2Cu_4O_8$ gives $T_\theta^{max}/T_c < 1$, which may reflect either uncertainties in the appropriate average of the a-axis and b-axis values of λ which

NJ=SC

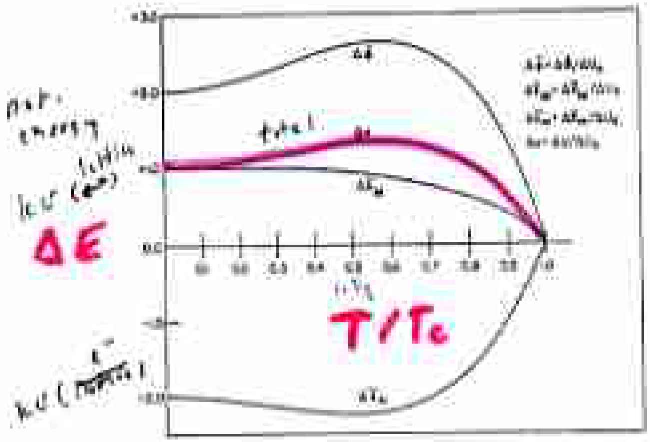

FIG. 1. The dependence of $\Delta\bar{k}_m$, $\Delta\bar{k}_M$, and $\Delta\phi$ on the reduced temperature $t=T/T_c$.

edge of the dependence of H_c on T, P, and M. This information is to be found from experiment. Secondly, we wish to point out that in this type of approach, which is by no means unknown in dealing with other physical phenomena, we reverse the usual order of procedure. Here we start from the experimental data, apply the general principles of statistical mechanics, and deduce some general results about the microscopic nature of the phenomenon. This is the reverse of the more usual procedure in which we start with some specific assumptions about the microscopic state, usually chosen so as to make the problem tractable, and then deduce with the aid of statistical mechanics some statements about the macroscopic behavior of the system.

2. CALCULATION OF THE DIFFERENCES $\Delta\bar{K}_m$, $\Delta\bar{K}_M$ AND $\Delta\bar{\Phi}$

Consider the Hamiltonian, H, for one mole of a pure isotope of any superconducting element. This can be written as

$$H=K_M+K_m+\Phi, \tag{2.1}$$

where

$$K_m=\sum_{i=1}^{ZN}\frac{\mathbf{p}_i^2}{2m}, \tag{2.2}$$

$$K_M=\sum_{i=1}^{N}\frac{P_i^2}{2M}, \tag{2.3}$$

and

$$\Phi=\sum_{i<j}^{N}\sum\frac{Z^2e^2}{|\mathbf{R}_i-\mathbf{R}_j|}-\sum_{i=1}^{N}\sum_{j=1}^{ZN}\frac{Ze^2}{|\mathbf{R}_i-\mathbf{r}_j|}+\sum_{i<j}^{ZN}\sum\frac{e^2}{|\mathbf{r}_i-\mathbf{r}_j|}. \tag{2.4}$$

In these equations, M and Z are the mass and atomic number of the isotope of the element concerned; m and e are the mass and charge of the electron. The momentum and coordinate of the ith nucleus are denoted by $\mathbf{P}_i$ and $\mathbf{R}_i$, while those of the ith electron are denoted by $\mathbf{p}_i$ and $\mathbf{r}_i$. The operators K_M, K_m, and Φ are the kinetic energy of electrons, kinetic energy of the nuclei and potential energy of the entire system. In writing down this Hamiltonian, we have assumed that the metal can be thought of as being composed of N nuclei of charge Ze and ZN electrons of charge e. This assumption seems to us to be perfectly sound.

Next we state the three general theorems of statistical mechanics that we require. First the internal energy, U, of the system is given by,

$$U=\bar{H}=\bar{K}_M+\bar{K}_m+\bar{\Phi}, \tag{2.5}$$

where $\bar{H}$ is the thermal average of the Hamiltonian H. The second theorem we shall need is the virial theorem.[3,4] This states that the product of the pressure, p, and volume, V, is given by

$$pV=\tfrac{2}{3}(\bar{K}_M+\bar{K}_m)+\tfrac{1}{3}\bar{\Xi}, \tag{2.6}$$

where $\bar{\Xi}$ is the average of the virial of the interparticle forces and is given by

$$\bar{\Xi}=-\sum_{i<j}^{N}\sum(\mathbf{R}_{ij}\cdot\nabla_{\mathbf{R}_{ij}}Z^2e^2/|\mathbf{R}_i-\mathbf{R}_j|)_{\mathrm{av}}+\sum_{i=1}^{N}\sum_{j=1}^{ZN}((\mathbf{R}_i-\mathbf{r}_j)\cdot\nabla_{(\mathbf{R}_i-\mathbf{r}_j)}Ze^2/|\mathbf{R}_i-\mathbf{r}_j|)_{\mathrm{av}}-\sum_{i<j}^{ZN}\sum(\mathbf{r}_{ij}\cdot\nabla_{\mathbf{r}_{ij}}e^2/|\mathbf{r}_i-\mathbf{r}_j|)_{\mathrm{av}}. \tag{2.7}$$

Now since the only interparticle forces present are Coulomb forces, it is easily seen that $\bar{\Xi}=\bar{\Phi}$. When this result is substituted into Eq. (2.6), we find that

$$\tfrac{3}{2}pV=\bar{K}_M+\bar{K}_m+\tfrac{1}{2}\bar{\Phi}. \tag{2.8}$$

Equations (2.5) and (2.8) are well-known results in statistical mechanics. Finally we shall use the following equation,

$$-M(\partial G/\partial M)_{P,T}=\bar{K}_M. \tag{2.9}$$

This equation, which is quite general, appears to be new and is derived in the appendix. A similar equation holds for the mean kinetic energy of the electrons, but we shall not require it. If we now express U and pV in terms of the derivatives of G, we find that Eqs. (2.5), (2.8), and (2.9) can be written in the form

$$-P\left[\frac{\partial G}{\partial P}\right]_{T,M}-T^2\left[\frac{\partial(G/T)}{\partial T}\right]_{P,M}=\bar{K}_M+\bar{K}_m+\bar{\Phi},$$

$$\tfrac{3}{2}P\left[\frac{\partial G}{\partial P}\right]_{T,M}=\bar{K}_M+\bar{K}_m+\tfrac{1}{2}\bar{\Phi},$$

and

$$-M\left[\frac{\partial G}{\partial M}\right]_{T,P}=\bar{K}_M.$$

---

[3] E. A. Milne, Phil. Mag. 50, 409 (1925).

[4] J. de Boer, Repts. Progr. Phys. 12, 305 (1948-19

IMPLICATIONS

High T_c Self-Consistency Loop

$$\begin{tikzcd}
 & \Delta(\mathbf{k},\omega) \arrow[dl] & \\
G(\mathbf{k},\omega) \arrow[dr] \arrow[rr] & & F_{NS}-F_{SC} \arrow[ul] \\
 & \chi(\mathbf{q},\omega) \arrow[ur] &
\end{tikzcd}$$

Dci- 9

This behavior can now be understood as arising from the narrowing of the resonance in energy from the normal to the superconducting states.

The temperature dependence of the resonance peak intensity [$S_{res}(q,\omega)$] for three $(123)O_{6+x}$ samples with different doping levels and transition temperatures is shown in Fig. 3, A through C. For $x = 0.6$, the temperature dependence of the momentum- and frequency-integrated resonance is found to be different from that of the peak intensity (Fig. 3A). For $(123)O_{6.8}$, similar behavior also occurs, but because the resonance is weaker above T_c, the counting times required to obtain reliable integrals of the type found for $x = 0.6$ are prohibitive, and so we are content with simply plotting the peak intensities. Finally, for $x = 0.93$, no broadening in either energy or wave vector has been identified (*1–5*), and so in this case, the temperature dependence of the integrated spectral weight does actually follow the peak intensity. We define the mean-squared (fluctuating) moment associated with the resonance as $\langle m^2_{res}\rangle = 3/(2\pi)\int d(\hbar\omega)\chi''_{res}(\omega)/[1 - \exp(-\hbar\omega/kT)]$, where $\hbar$ is Planck's constant divided by 2π, k is Boltzmann's constant, $\chi''_{res}(\omega)$ (*14, 15*) is the resonance part of the acoustic spectrum of Fig. 1, and the factor of 1/2 arises from averaging $\sin^2(q_z d/2)$ over q_z. For $(123)O_{6.6}$ and $(123)O_{6.93}$, our measurements are expressed in absolute units obtained by scaling to the low-temperature measurements performed on both compounds at ISIS (*13*).

The most obvious feature of Fig. 3, A through C, is that as the doping level and T_c decrease, there is a progressively larger pretransitional regime above T_c. Specifically, for the ideally doped sample ($x = 0.93$), the onset of the resonance occurs at a temperature T^* which almost coincides with T_c. For $x = 0.8$ and 0.6, T^* increases to approximately 115 ± 15 and 150 ± 20 K, respectively, even while both T_c and the resonance energy itself are reduced. Thus, the weight of the temperature-dependent resonance joins the long list of properties that show pretransitional behavior in suboptimally doped $(123)O_{6+x}$. The cross-over temperature T^* (Fig. 4A) coincides with the temperatures below which the temperature derivatives of the electrical resistivity $d\rho(T)/dT$ (*19, 20*) and the Cu nuclear $(T_1T)^{-1}$ relaxation rate (*21*) reaches a broad maxima. The anomalies occurring at T^* are generally associated with the opening of a pseudogap in the low-energy spin excitation spectrum, a supposition also supported by neutron scattering data such as those in Fig. 1.

According to thermodynamics, a metal undergoes a transition into the superconducting state because such a transition can lower its total free energy, F (*22*). The difference in free energy of the system between the normal state, extrapolated to zero temperature (F_N) and the superconducting state (F_S) is the condensation energy, that is, $E_C = (F_N - F_S)_{T=0}$. In principle, the free energy of a system, and therefore E_C, can be derived from the temperature dependence of $C^{el}(x,T)$ (*8*). For $(123)O_{6+x}$, $C^{el}(x,T)$ has been measured by Loram *et al.* (*9*). The key features of the corresponding data (Fig. 3E) are a sharp jump at T_c for the optimally doped $(123)O_{6.92}$, which becomes much suppressed upon reduction of the oxygen content. Although there is less entropy released at T_c, more seems to be released at temperatures above T_c, as x is reduced below its optimal value. Thus, the specific heat tracks the temperature derivative (Fig. 3D) of the spectral weight of the resonance. Just as for the specific heat, decreasing doping reduces the maximum in $d\langle m^2_{res}\rangle/dT$ at T_c and introduces progressively broader high-temperature tails.

In the $t - J$ model (*23*), the Hamiltonian of the system consists of a nearest-neighbor

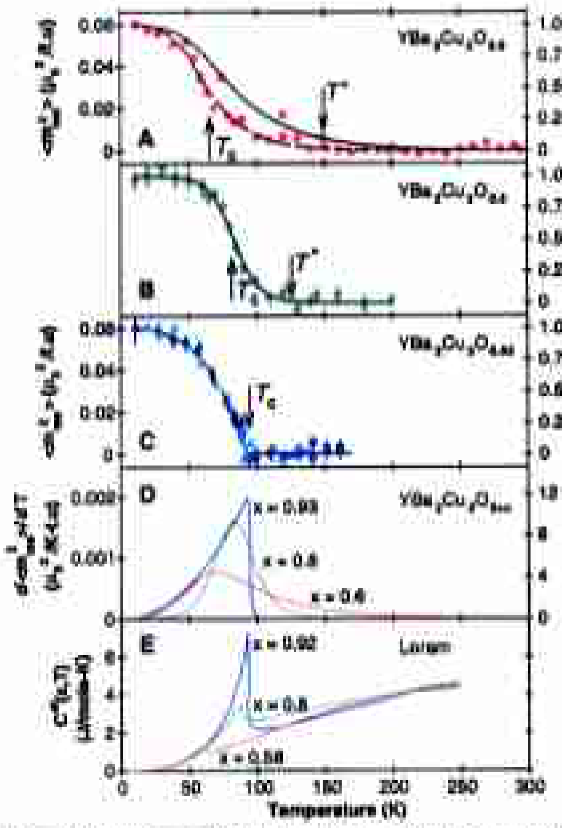

Fig. 3. Temperature dependence of the resonance peak intensity (circles) for (A) $(123)O_{6.6}$ at $\hbar\omega$ = 34 meV, (B) $(123)O_{6.8}$ at 39 meV, and (C) $(123)O_{6.93}$ at 40 meV at the (0.5,1.5,1.7) rlu position on triple-axis spectrometers at HFIR. Left axes show intensity normalized to $\langle m^2_{res}\rangle$ and right axes to the peak intensity at low temperatures. The error bars in (A) through (C) include only the statistical errors of the triple-axis measurements. The squares in (A) are the integrated $S_{res}(q,\omega)$ and the triangles in (C) are from (*2*). The T^* values are defined as the initial appearance of the resonance. The solid line in (C) below T_c is a fit using the modified two-fluid model $I(T)/I(0) = 1 - (T/T_c)^{5.09}$. (D) The estimated $d\langle m^2_{res}\rangle/dT$ for $(123)O_{6+x}$ is from the temperature derivative of the solid lines in (A) through (C). To calculate the absolute magnitude of $C^{res}_J(x,T)$ using Eq. 2, we assumed J = 125 meV (*13*), $\langle m^2_{res}\rangle$ = 0.06 $\mu_B{}^2$f.u.$^{-1}$, and 1 mol = 666.15 g for each of the three compositions. Note, we have not considered the uncertainties of $C^{res}_J(x,T)$ arising from the systematic errors in determining the absolute magnitude of $\langle m^2_{res}\rangle$, due most notably to the ambiguity in removing the nonresonance portion of the signal (Fig. 1A). (E) $C^{el}(x,T)$ from (*9*) was converted to SI units using 1 gram-atom unit = 1/(12 + x) moles.

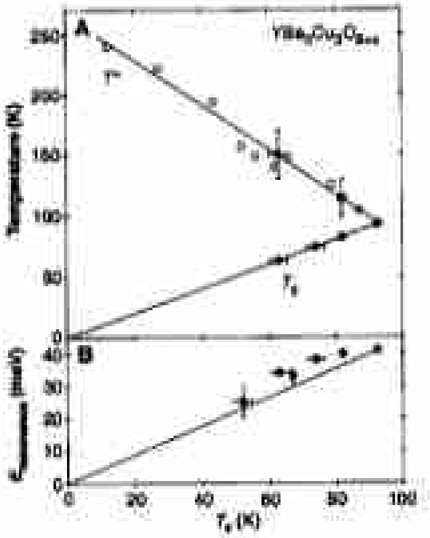

Fig. 4. Phase diagram of $(123)O_{6+x}$, which summarizes the results of transport, NMR, and neutron scattering. Because of various methods of oxygenation, slightly different T_c values are reported for the same nominal doping of $(123)O_{6+x}$. We avoid this inconsistency by plotting characteristic temperatures as a function of T_c. (A) The open circles and open squares are temperatures at which $d\rho(T)/dT$ reaches a broad maximum (*19, 20*). The open diamonds show the pseudogap temperature T^* determined from NMR measurements (*21*). The filled circles locate T_c and T^*, where the resonance first appears in our samples. (B) Filled circles show resonance energy versus the transition temperature T_c. Filled squares are from Fong *et al.* (*5*). Horizontal error bars are superconducting transition widths. The solid lines are guides to the eye.

Change in Internal Energy Between Normal and Superconducting States

$$U_N - U_S =$$

$$\Sigma_{\mathbf{k}} \int d\omega\, (\omega + \varepsilon_{\mathbf{k}})\, f(\omega)\, [A_N(\mathbf{k},\omega) - A_S(\mathbf{k},\omega)]$$

$$= \Sigma_{\mathbf{k}}\, \varepsilon_{\mathbf{k}}\, [n_N(\mathbf{k}) - n_S(\mathbf{k})]$$

$$+ \int d\omega\, \omega\, f(\omega)\, [N_N(\omega) - N_S(\omega)]$$

where

A is the spectral function
ε is the dispersion
f is the Fermi function
n is the momentum distribution
N is the density of states

Kinetic Energy - $(2\varepsilon_k)$
Potential Energy - $(\omega - \varepsilon_k)$

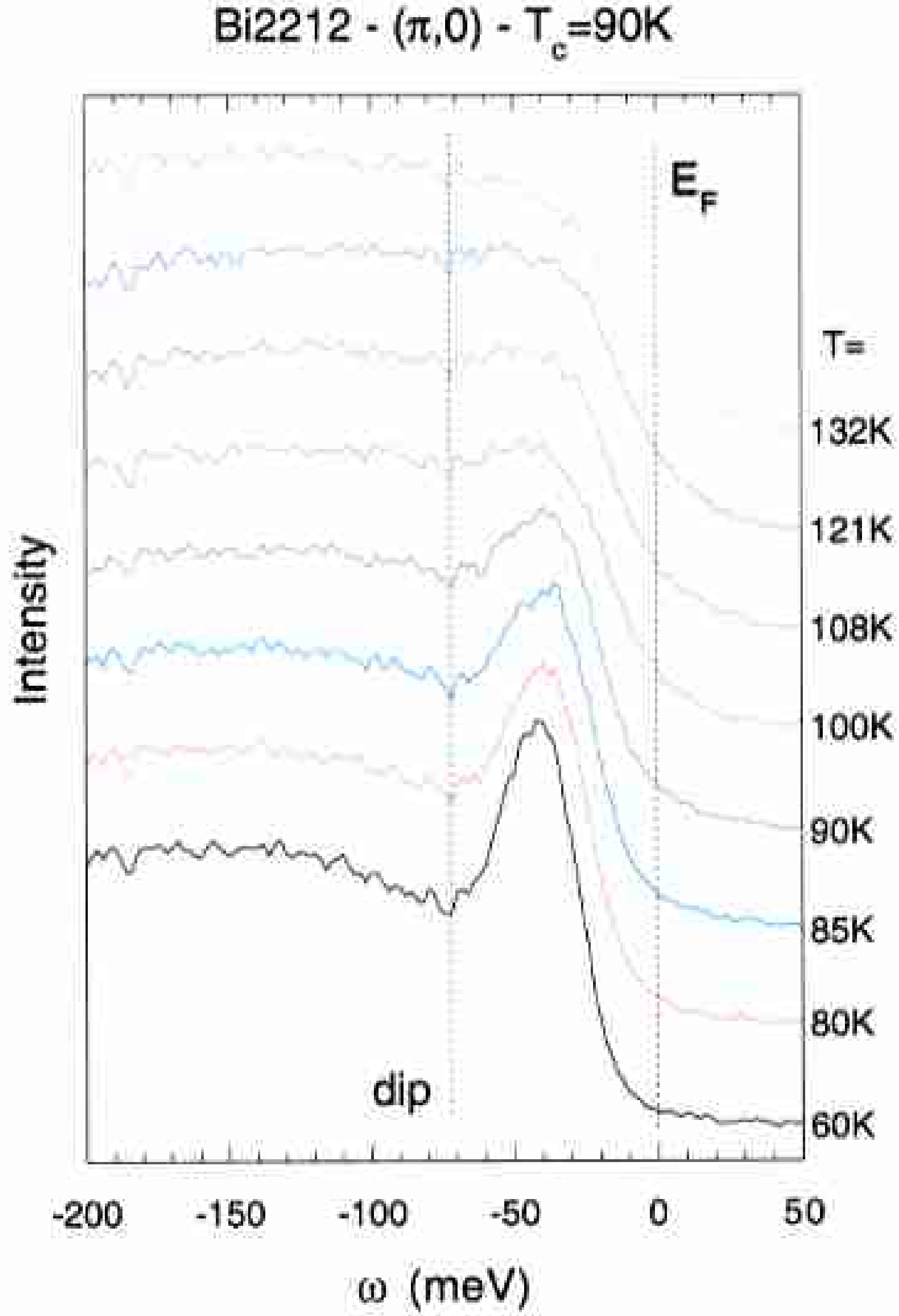
Bi2212 - (π,0) - T$_c$=90K
E$_F$
T=
132K
121K
108K
100K
90K
85K
80K
60K
Intensity
dip
-200
-150
-100
-50
0
50
ω (meV)

ARPES spectrum above and below T_c at $(\pi,0)$ for Bi2212

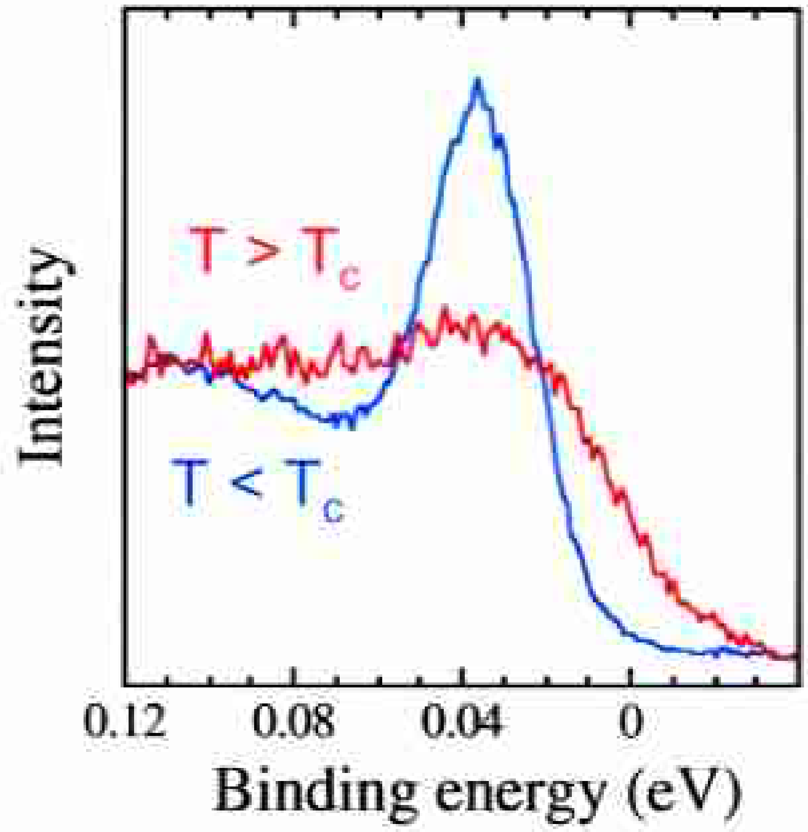

Self energy from interaction with a bosonic spectrum red is above T_c, blue below, with a collective mode inside gap

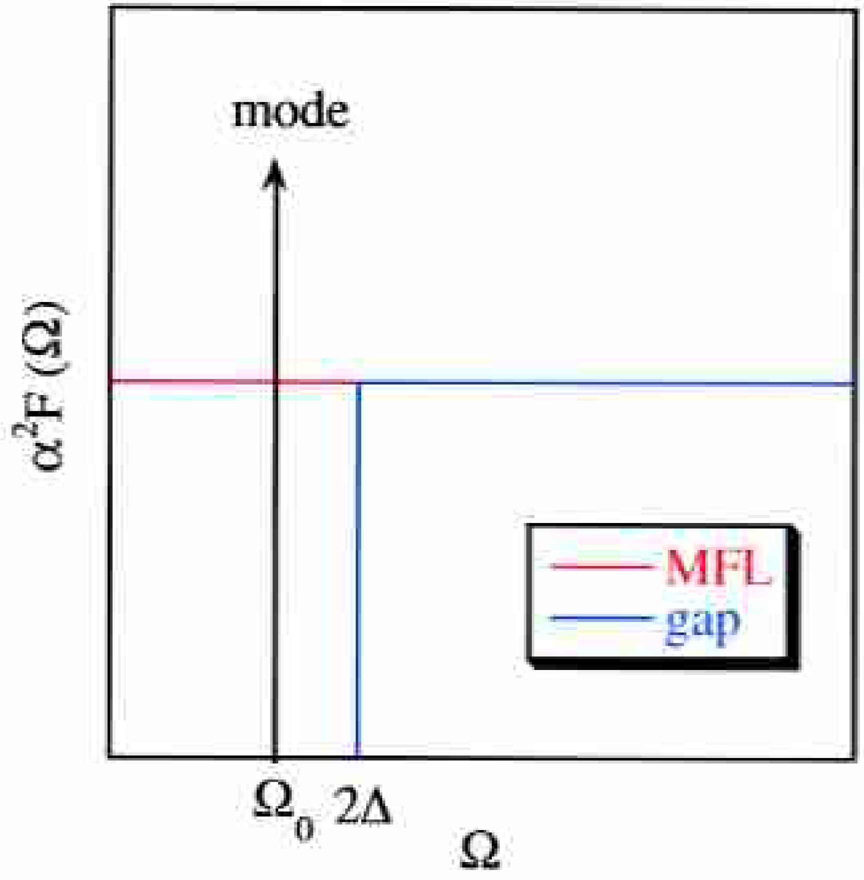

Feynman diagram leading to left picture, α^2F is the spectral function of bubble

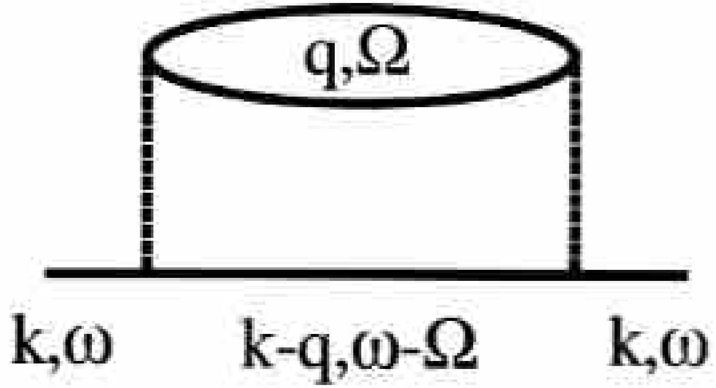

Neutron Data

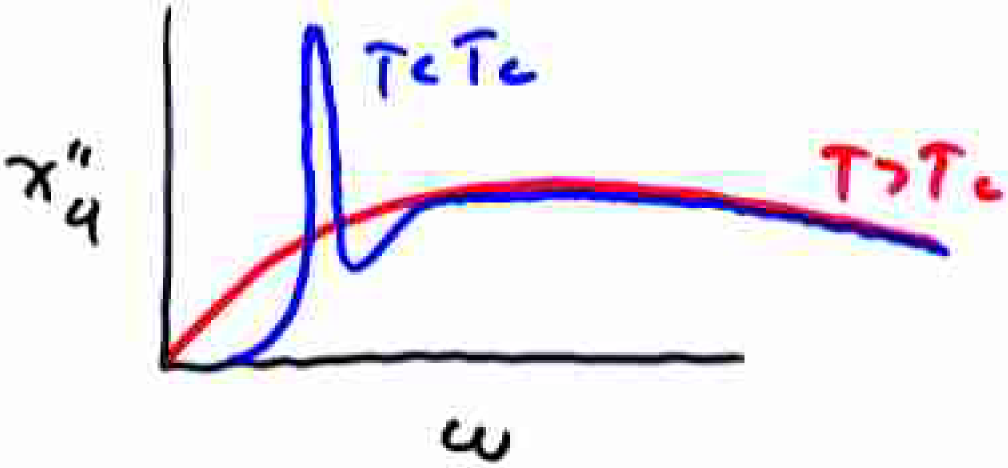

$Q = (\pi, \pi, \pi)$, $S = 1$

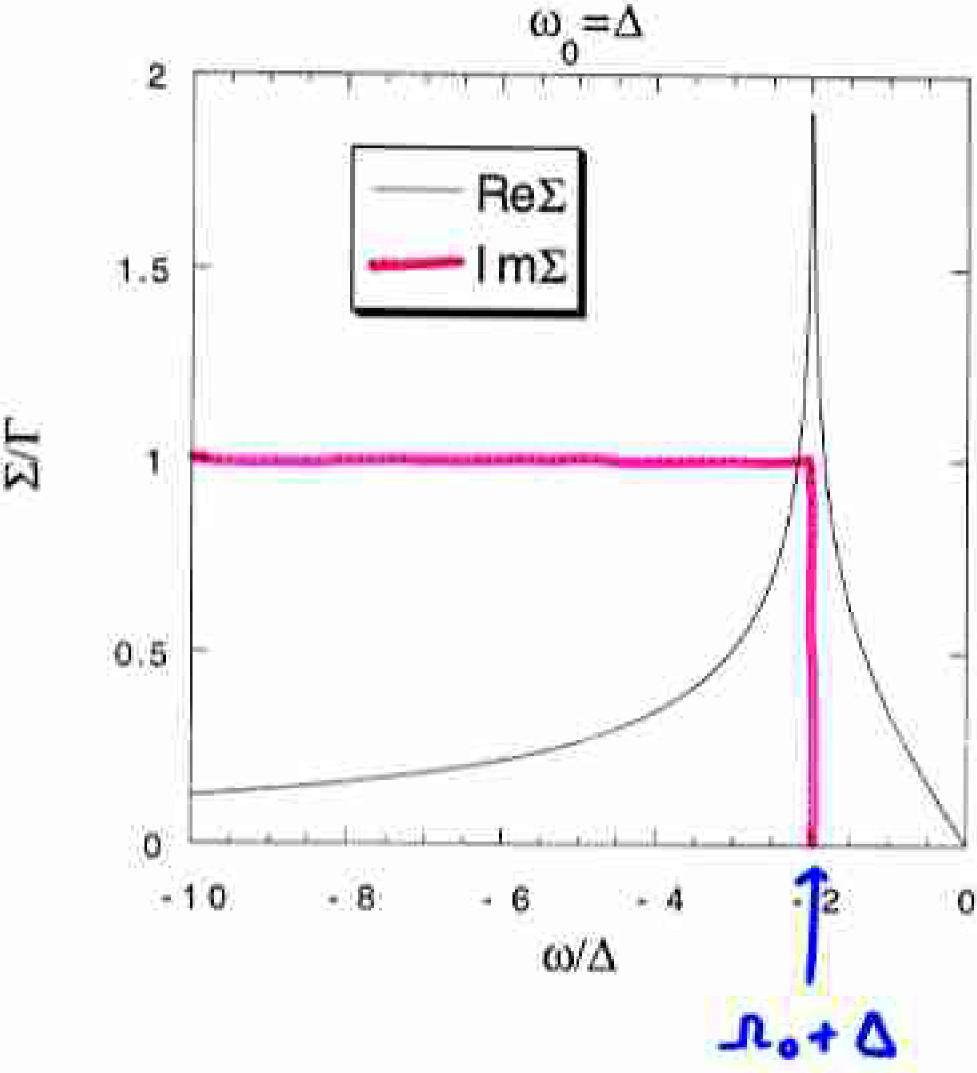
$\omega_0=\Delta$
ReΣ
ImΣ
Σ/Γ
2
1.5
1
0.5
0
-10
-8
-6
-4
-2
0
ω/Δ
$\Omega_0+\Delta$

Top - Self energy in superconducting state (mode energy Ω_0)
Bottom - Theory spectra (blue) compared to experiment (red)

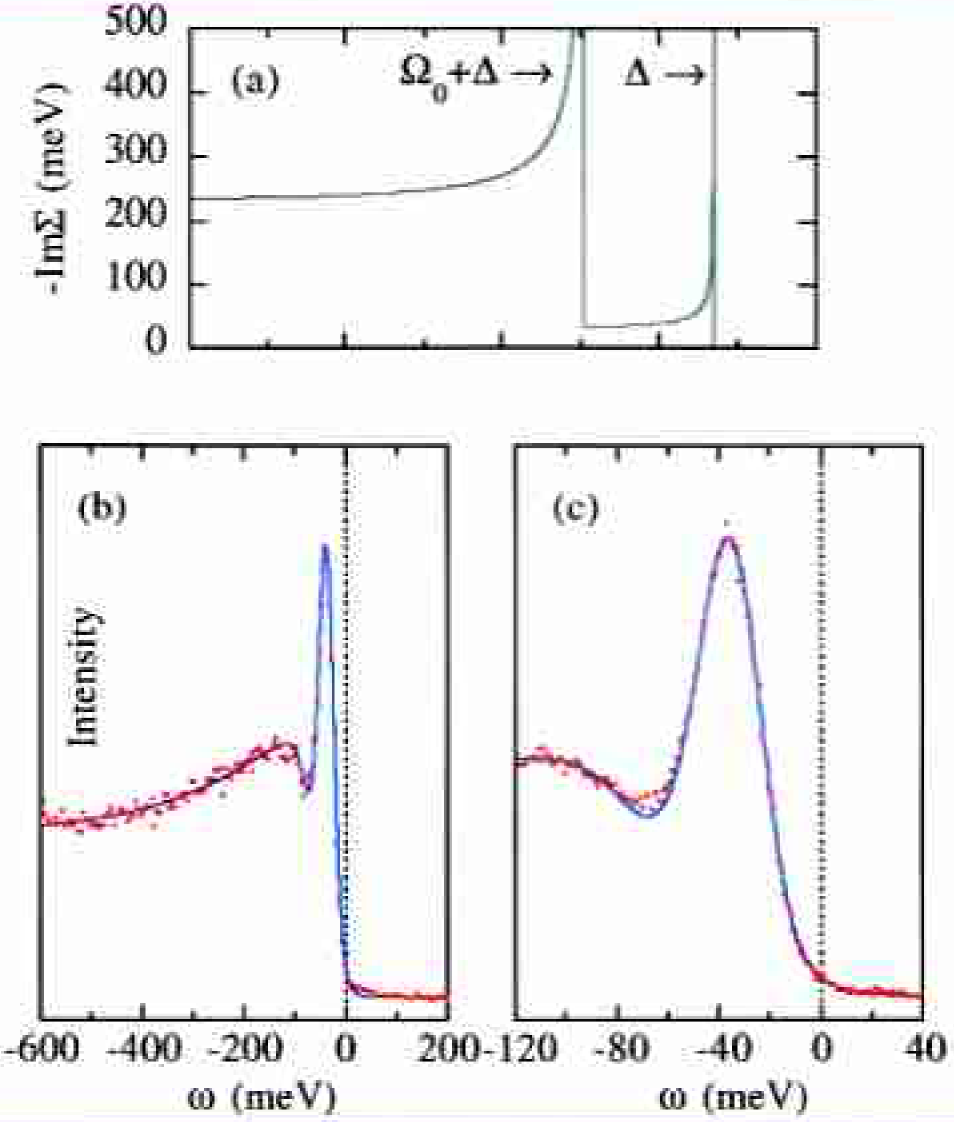

ARPES data (dip minus peak energy) versus doping compared to mode energy from neutron scattering data

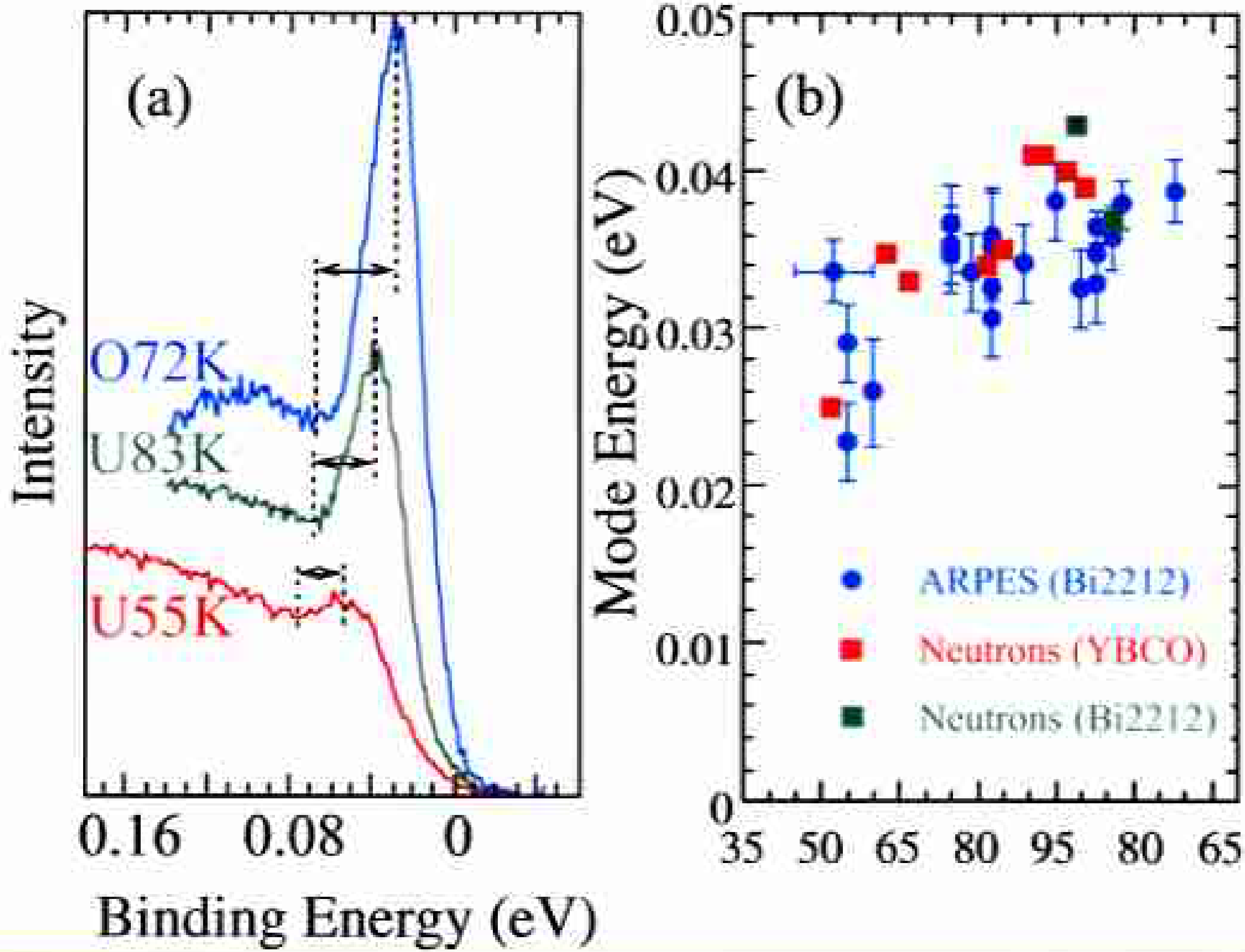

Mode energy from tunneling (Zasadzinski/Gray) versus doping
The doping dependence tracks both ARPES and neutron data

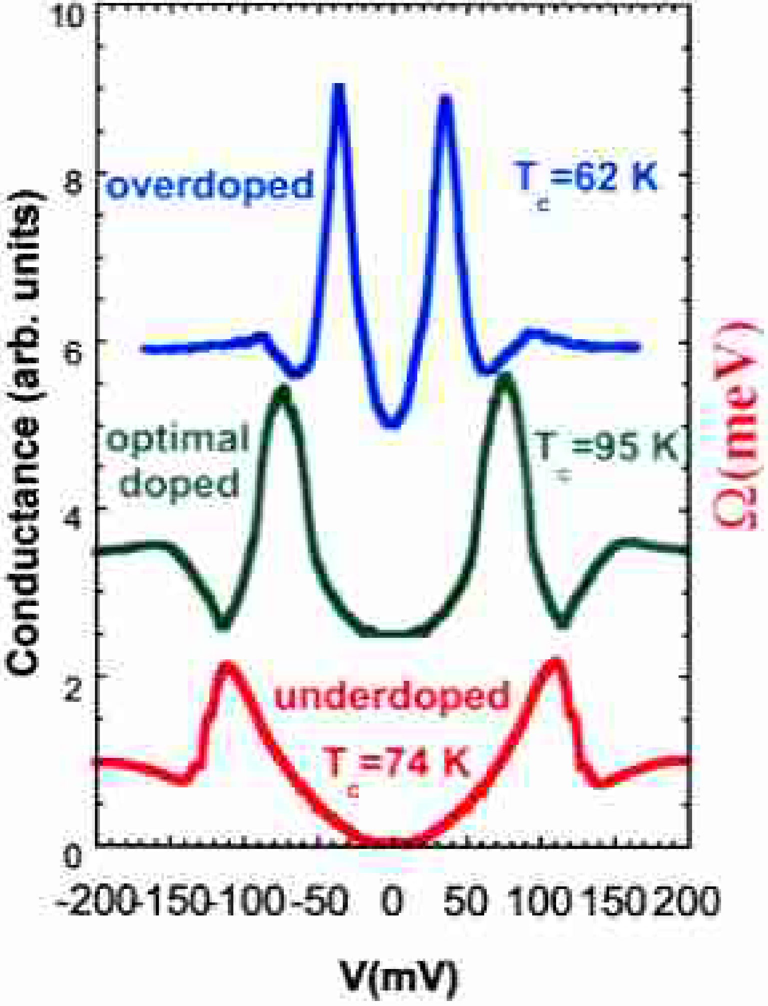

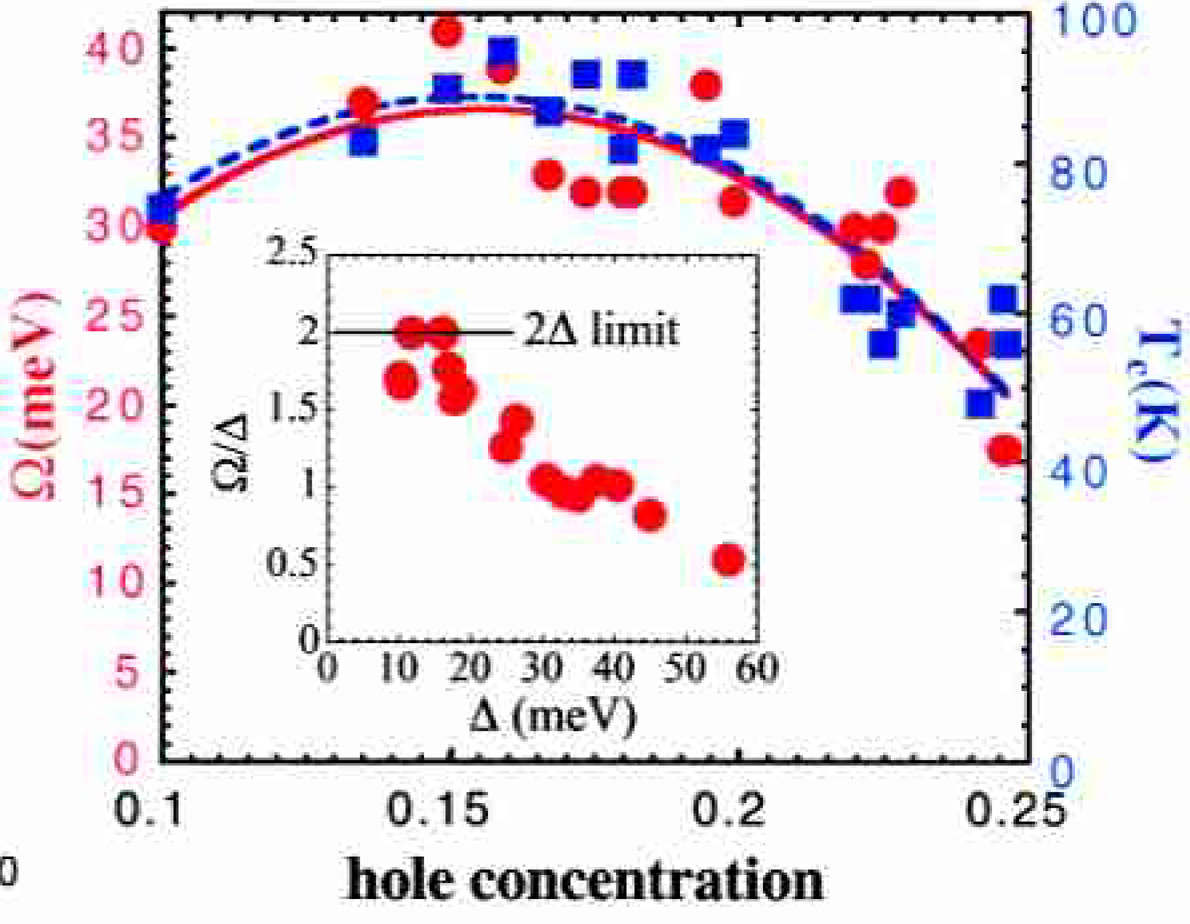

PRL **87**, 067005 (2001)

PRB Jun 0

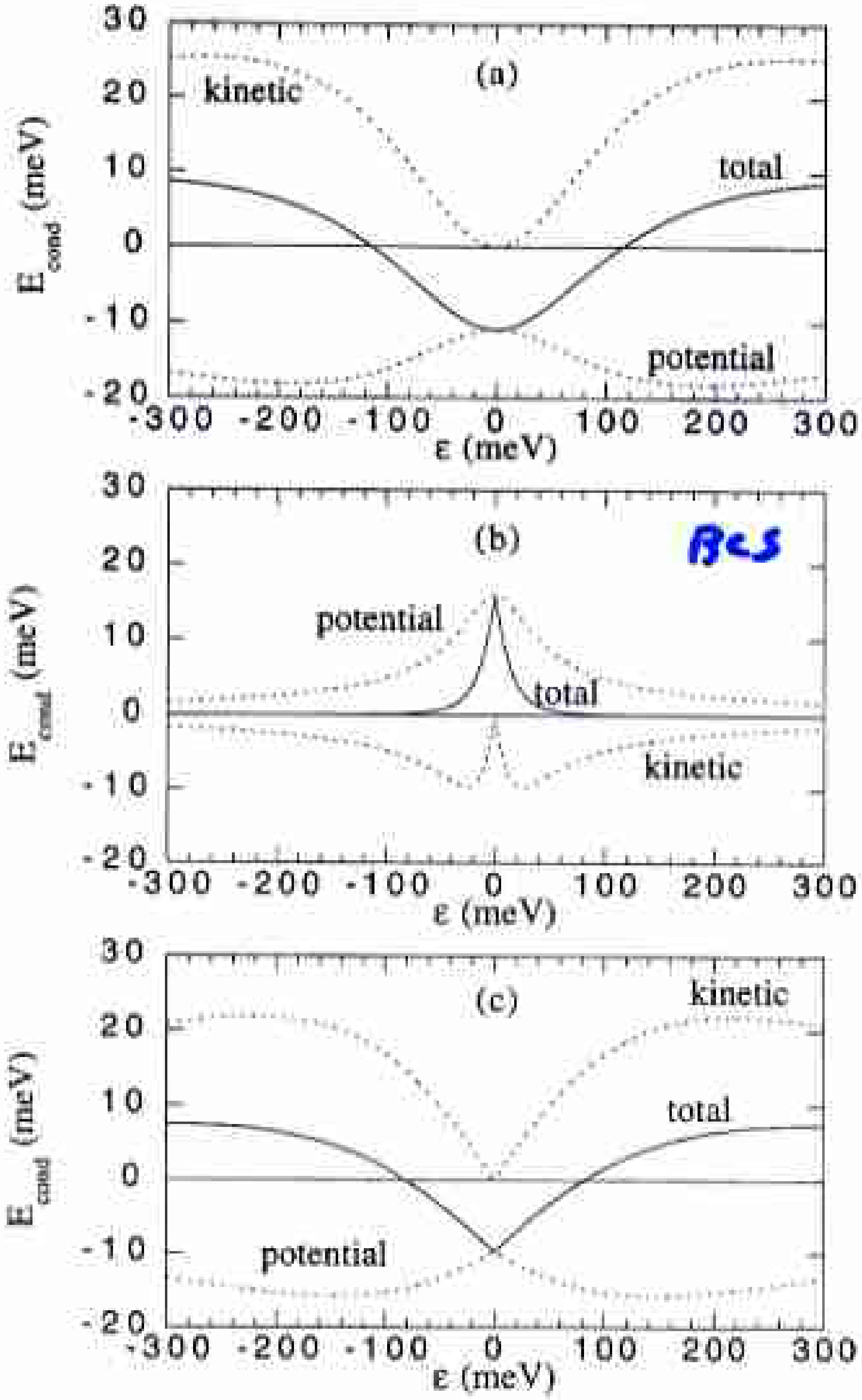
(a)
kinetic
total
potential
E_{cond} (meV)
30
20
10
0
-10
-20
-300
-200
-100
0
100
200
300
ε (meV)
(b)
BCS
potential
total
kinetic
E_{cond} (meV)
30
20
10
0
-10
-20
-300
-200
-100
0
100
200
300
ε (meV)
(c)
kinetic
total
potential
E_{cond} (meV)
30
20
10
0
-10
-20
-300
-200
-100
0
100
200
300
ε (meV)

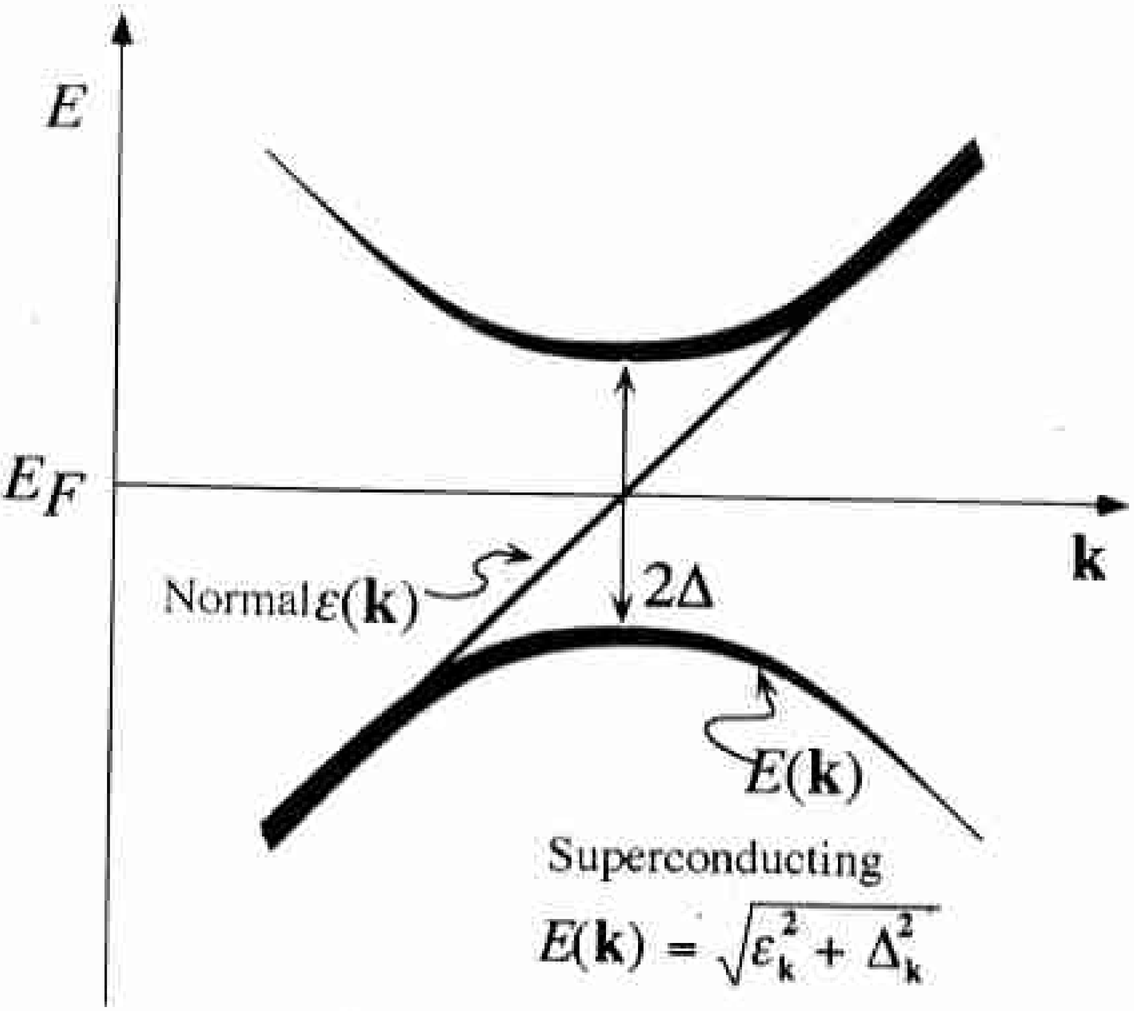E
E_F
$\mathbf{k}$
Normal $\varepsilon(\mathbf{k})$
2Δ
$E(\mathbf{k})$
Superconducting
$E(\mathbf{k}) = \sqrt{\varepsilon_{\mathbf{k}}^2 + \Delta_{\mathbf{k}}^2}$

Momentum distribution from mode model for normal state (red) and superconducting one (blue). Trend is opposite BCS theory

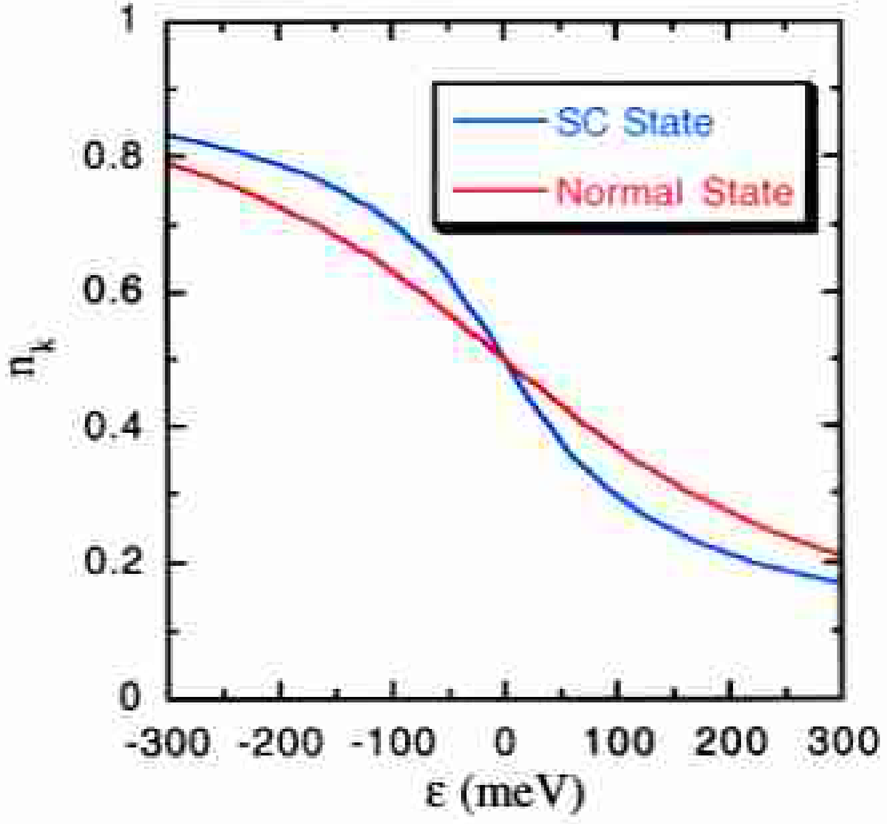

PRB Jun 00

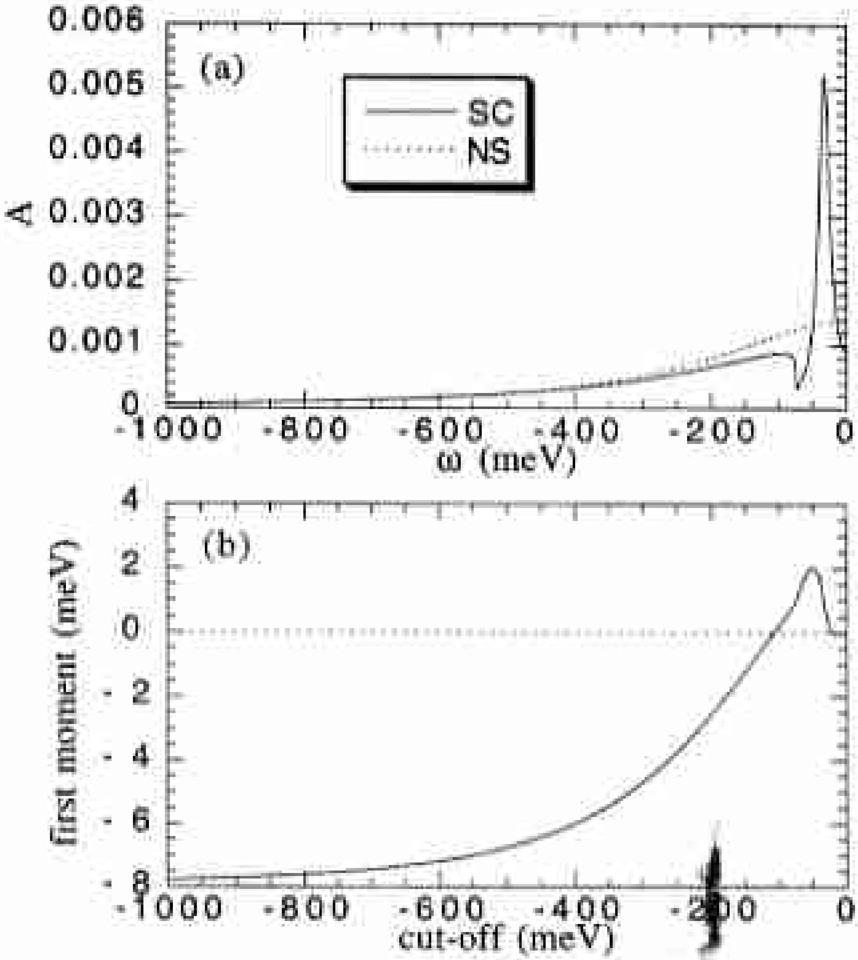

(a)
SC
NS
A
0.006
0.005
0.004
0.003
0.002
0.001
0
-1000
-800
-600
-400
-200
0
ω (meV)
(b)
first moment (meV)
4
2
0
- 2
- 4
- 6
- 8
-1000
-800
-600
-400
-200
0
cut-off (meV)

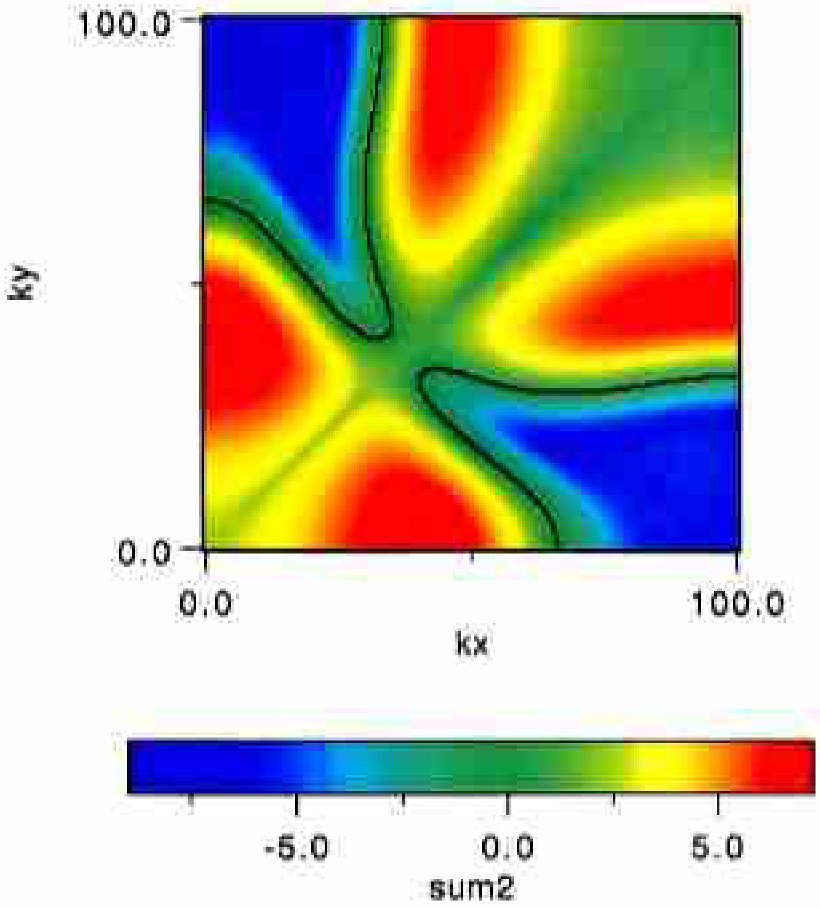

sum2_3 vs. (row, col)

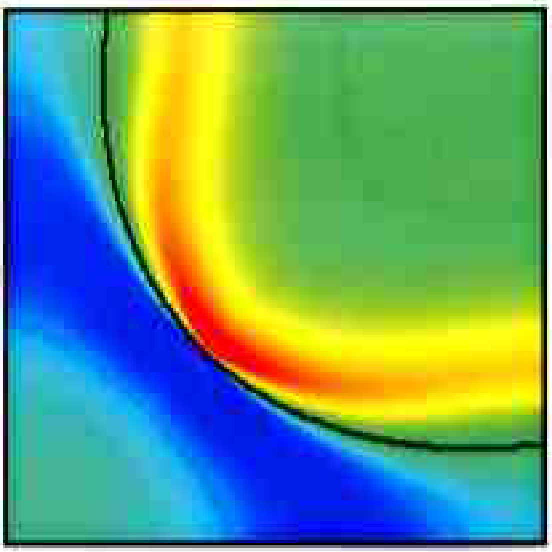

Δn_k

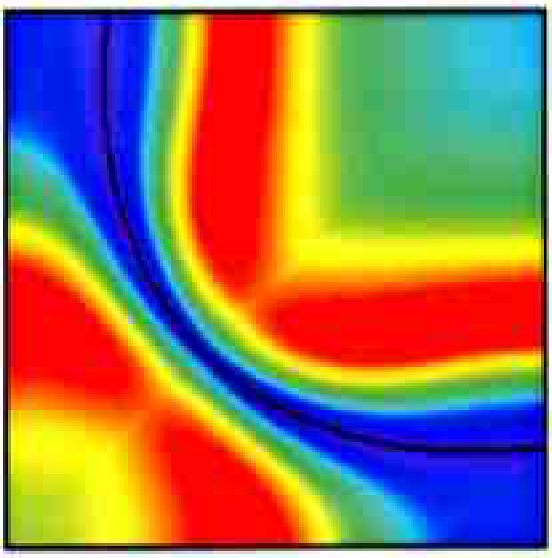

ΔE_{kin}

$$\int_0^\infty Re\sigma_{xx}(\omega)d\omega = \frac{\pi e^2 a^2}{2\hbar^2 V} E_K$$

$$E_K = \frac{2}{a^2 N} \sum_k \frac{\partial^2 \epsilon_k}{\partial k_x^2} n_k$$

$$E_{kin} = \frac{2}{N} \sum_k \epsilon_k n_k$$

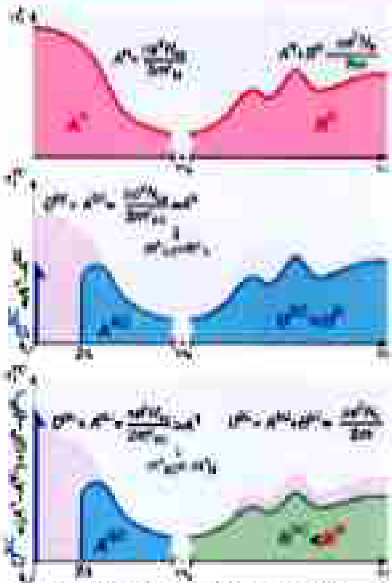

Summing up. Relations between the fundamental and partial sum rules (**top**). For conventional superconductors, the effective mass is preserved through the superconducting transition that leads to the Ferrell-Glover-Tinkham sum rule (**middle**). The latter is violated for *c*-axis conductivity in the cuprate superconductors, where, as a result of delocalization of carriers at temperatures below T_c, the strength of the zero frequency δ function gains only about half of its spectral weight from intraband transitions *A* and the remainder from interband transitions *B* (**bottom**).

(Return to Article)

Volume 283, Number 5398, Issue of 1 Jan 1999, p. 43.

PAGE TOP

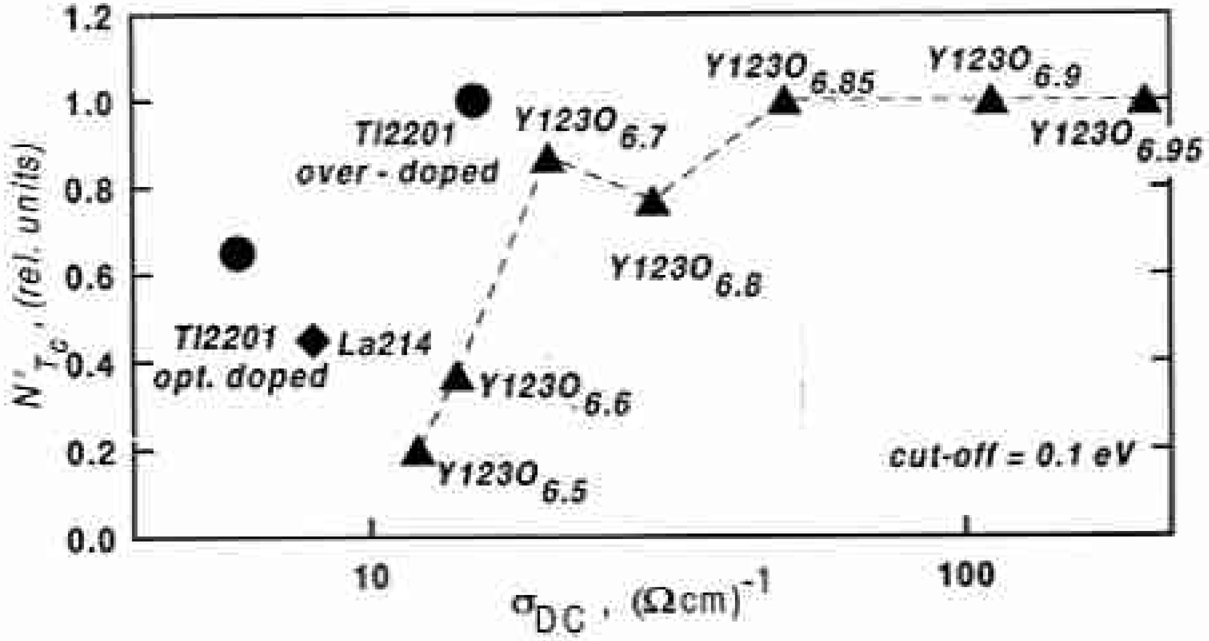

Fig.3
"Unconventional energetics ..."
Basov et al.

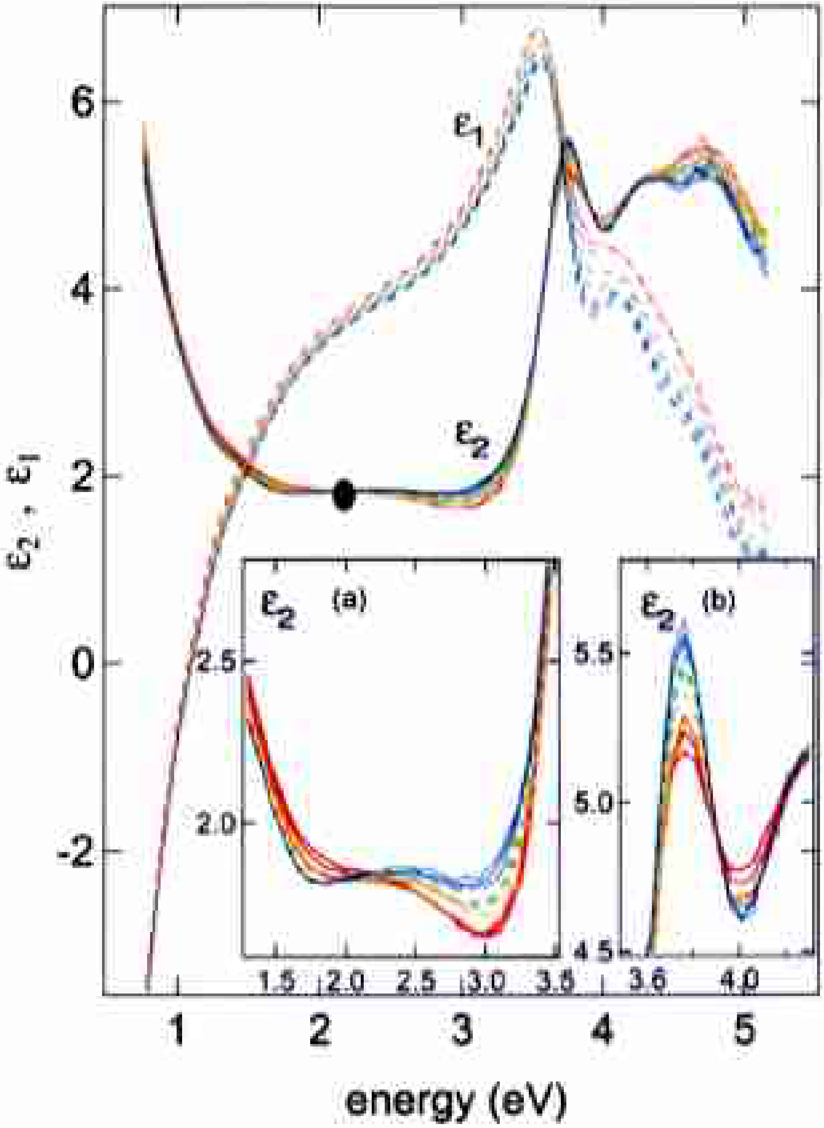

FIG. 1. (Color) Real (dashed lines) and imaginary part (solid lines) as a function of temperature. The inset enlarges the most important spectroscopic regions in ϵ_2 from 1.4 to 3.5 eV (a) and from 3.6 to 4.3 eV (b). In the insets thick red solid, yellow and green dashed, and blue thin solid lines denote the temperature ranges from 300 to 170 K, 170 to 100 K, and below 90 K.

when correcting for the window strain effects, as the samples move relative to the window due to a contracting coldfinger and the strain field is a function of the area through which the light penetrates in order to hit the sample. Therefore we were limited in our temperature-dependent study to the two large crystals discussed in the following. By estimating the room-temperature plasma frequency from the pseudodielectric ϵ_1, we can confirm that the overdoped crystal shows a plasma frequency which is about 7% higher than that of the underdoped sample.

III. RESULTS AND DISCUSSION

In Fig. 1 we show the pseudodielectric function $\epsilon = \epsilon_1 + i\epsilon_2$ for the underdoped crystal as a function of photon energy for several temperatures. One can observe in ϵ_1 a slight shift of the plasma frequency towards higher energies with decreasing temperature, which is mostly a consequence of lattice contraction and the corresponding enhancement of the carrier density. In ϵ_2, we find a crossing point at around 2.2 eV separating this carrier dominated frequency region from a higher frequency region which is dominated by interband transitions related to the Cu-O and Bi-O bands.[13] The charge-transfer gap being clearly visible in nonsuperconducting compounds at 1.7 eV weakens with increasing doping and vanishes as the Drude response develops in the metallic state of the cuprates. The *a/b*-plane anisotropy of the peak around 3.8 eV in ϵ_2 indicates that its origin is due to interband transitions involving the Bi-O bands, which show typical *a/b* anisotropy due to the superlattice distortions in the Bi-O layers.[13,18] The other transitions at energies between 2.5 and 5 eV hardly show any anisotropy effects and have to be related to the Cu-O and possibly the Bi-O layers. However, it is quite remarkable that Kelly *et al.* have found transitions at 4 and 5 eV in CuO_2, $CrCuO_2$, $Ca_{1.8}Sr_{0.2}Cu_2O_4$, and $BaCuO_2$, which do not contain Bi-O planes.[13] Similar transitions can be found in $YBa_2Cu_3O_7$.[1,2,12] Linear muffin-tin orbital (LMTO) local-density approximation (LDA) calculations suggest in agreement with the experimental find-molegraaf-o

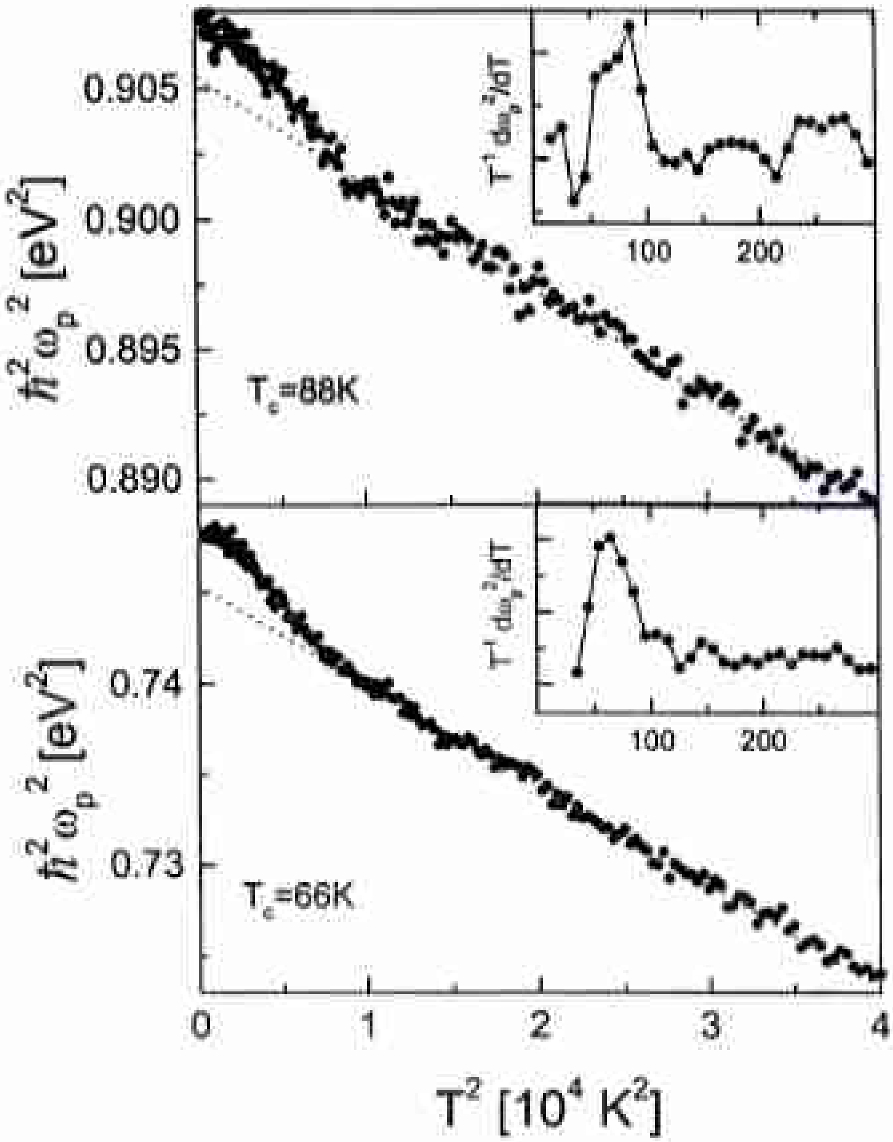

Figure 2 Temperature dependence of the screened plasma frequency ω_p^2 for optimally and underdoped $Bi_2Sr_2CaCu_2O_{8+\delta}$. Insets: derivaties $T^{-1}d\omega_p^2/dT$.

Molegraaf-o

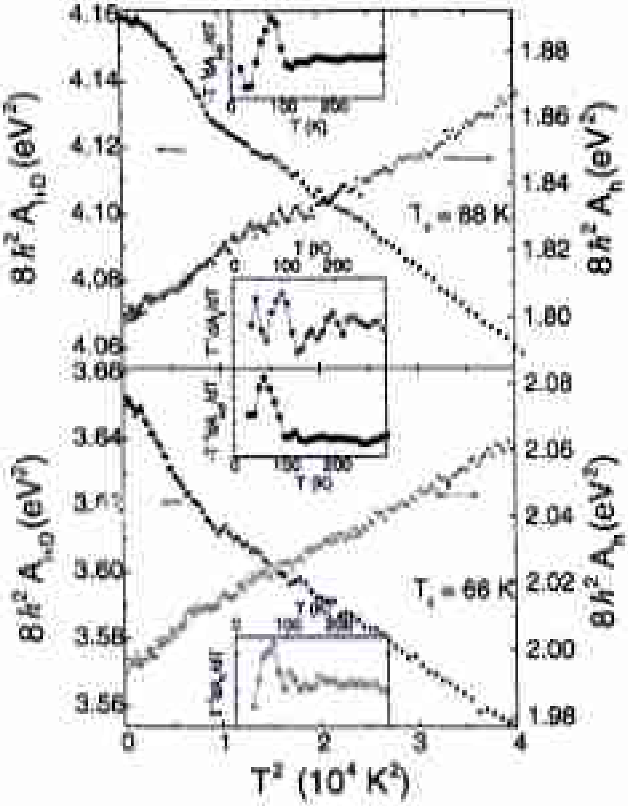

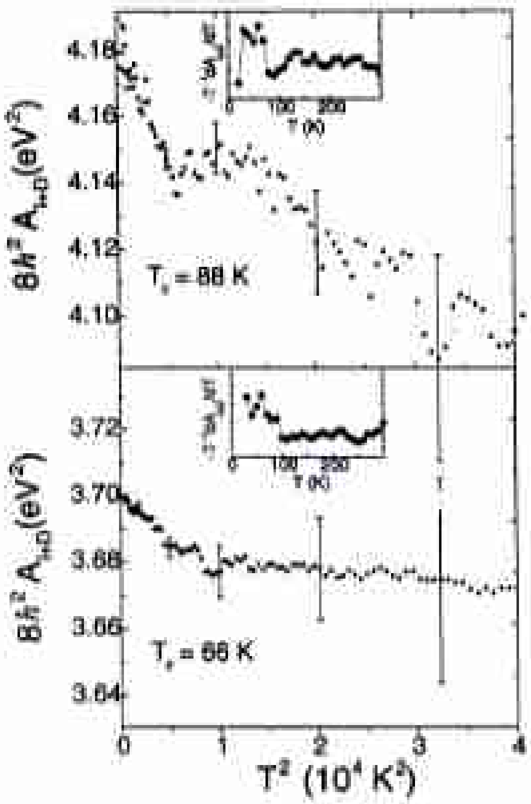

Fig. 3 (left). Temperature dependence of the low-frequency spectral weight $A_{l,D}(T)$ and the high-frequency spectral weight $A_h(T)$, for optimally doped (top) and underdoped (bottom) $Bi_2Sr_2CaCu_2O_{8+\delta}$. **(Insets)** Derivatives $-T^{-1}dA_{l,D}/dT$ and $T^{-1}dA_h/dT$. **Fig. 4 (right).** Temperature dependence of the low-frequency spectral weight $A_{l,D}(T)$ for optimally doped (top) and underdoped (bottom) $Bi_2Sr_2CaCu_2O_{8+\delta}$. The infrared optical conductivity was obtained by a Kramers-Kronig transformation of the reflection data. **(Insets)** Derivatives $-T^{-1}dA_{l,D}/dT$.

depending on the doping (34). The question of whether the observed spectral weight transfer is a generic property of the cuprates or a specific property of $Bi_2Sr_2CaCu_2O_{8+\delta}$ needs to be addressed by further experiments.

We see that in underdoped and optimally doped $Bi_2Sr_2CaCu_2O_{8+\delta}$ the onset of superconductivity is accompanied by a transfer of spectral weight from the visual region above 10,000 cm^{-1} to the intraband optical spectrum. This behavior contradicts that expected from traditional models of superconductivity and is a strong indication that superconductivity in the cuprates is unconventional.

References and Notes

1. M. Tinkham, *Introduction to Superconductivity* (McGraw-Hill, New York, ed. 2, 1996).
2. S. Chakravarty, A. Sudbø, P. W. Anderson, S. Strong, *Science* **261**, 337 (1993).
3. P. W. Anderson, *Science* **268**, 1154 (1995).
4. J. E. Hirsch, *Physica C* **199**, 305 (1992).
5. ———, *Physica C* **201**, 347 (1992).
6. F. F. Assaad, M. Imada, D. J. Scalapino, *Phys. Rev. Lett.* **77**, 4592 (1996).
7. P. A. Lee, *Physica C* **317**, 194 (1999).
8. P. W. Anderson, *Physica C* **341-348**, 9 (2000).
9. V. J. Emery, S. A. Kivelson, *J. Phys. Chem. Solids* **61**, 467 (2000).
10. S. Alexandrov, N. F. Mott, *High Temperature Superconductors and Other Superfluids* (Taylor and Francis, London, 1994).
11. D. van der Marel, J. Schützmann, H. S. Somal, J. W. van der Eb, in *Proceedings of the 10th Anniversary HTS Workshop on Physics, Materials & Applications* (USA World Scientific Publishers, River Edge, NJ), pp. 357–370.
12. A. J. Leggett, *Science* **274**, 587 (1996).
13. K. A. Moler, J. R. Kirtley, D. G. Hinks, T. W. Li, M. Xu, *Science* **279**, 1193 (1998).
14. P. W. Anderson, *Science* **279**, 1196 (1998).
15. A. A. Tsvetkov *et al.*, *Nature* **395**, 360 (1998).
16. D. N. Basov *et al.*, *Science* **283**, 49 (1999).
17. L. Feng *et al.*, *Science* **289**, 277 (2000).
18. H. Ding *et al.*, *Phys. Rev. Lett.* **87**, 227001 (2001).
19. M. V. Klein, G. Blumberg, *Science* **283**, 42 (1999).
20. M. A. Quijada *et al.*, *Phys. Rev. B* **60**, 14917 (1999).
21. D. Tanner *et al.*, *Physica B* **244**, 1 (1998).
22. I. Fugol *et al.*, *Solid State Commun.* **86**, 385 (1993).
23. Y. Yagil, E. K. H. Salje, *Physica C* **256**, 205 (1996).
24. M. J. Holcomb, J. P. Collman, W. A. Little, *Phys. Rev. Lett.* **73**, 2360 (1994).
25. S. G. Han, Z. V. Vardeny, K. S. Wong, O. G. Symko, G. Koren, *Phys. Rev. Lett.* **65**, 2708 (1990).
26. C. J. Stevens *et al.*, *Phys. Rev. Lett.* **78**, 2212 (1997).
27. M. Rübhausen, A. Gozar, M. V. Klein, P. Guptasarma, D. G. Hinks, *Phys. Rev. B* **63**, 224514 (2001).
28. The crystals were 1 by 3 mm in size and 0.1 mm in thickness, with mirror-like *ab* planes, and were grown by the traveling solvent floating zone method in an argon/oxygen mixture. Underdoped crystals were obtained by annealing in flowing nitrogen at 700°C and optimally doped crystals were obtained by annealing in flowing air at 750°C for several days. Between 6000 and 36,000 cm^{-1}, the *ab*-plane pseudodielectric function was measured with spectroscopic ellipsometry, at an angle of incidence of 80° and a pressure below 2×10^{-8} mbar. The pseudodielectric functions were then corrected for the admixture of *c*-axis polarization by means of *c*-axis optical constants [see also S. Tajima, G. D. Gu, S. Miyamoto, A. Odagawa, N. Koshizuka, *Phys. Rev. B* **48**, 16164 (1993)].
29. J. W. van der Eb, A. B. Kuz'menko, D. van der Marel, *Phys. Rev. Lett.* **86**, 3407 (2001).
30. The overall temperature dependence appears to be somewhat different for the two methods. Ellipsometry measures relative amplitudes for different polarizer settings and is therefore self aligned. Reflectometry is more strongly affected by instrumental drift. The error bars in Fig. 4 indicate the range within which the traces as a function of temperature of method (ii) can vary due to a gradual drift of the detected signal.
31. M. R. Norman, C. Pépin, preprint available at http://xxx.lanl.gov/abs/cond-mat/0201415 (2002).
32. Modeling the valence band with a nearest neighbor (*t*) and a next-nearest neighbor (*t'*) hopping term, and adopting $t'/t = 0.3$ for $Bi_2Sr_2CaCu_2O_{8+\delta}$, we have verified that the intraband spectral weight is given by Eq. 2 with a variation around the Fermi surface within ~20% [see also E. Pavarini, I. Dasgupta, T. Saha-Dasgupta, O. Jepsen, O. K. Andersen, *Phys. Rev. Lett.* **87**, 047003 (2001)].
33. By extrapolating the normal state $A_l^n(T)$ to 4 K, the difference spectral weight, $\Delta A_l = A_{l,s}(4\ K) - A_l^n(4\ K)$, can be calculated. To make the conversion from the units of eV^2 used in Fig. 3 to units of meV per Cu atom, we have to multiply $8\hbar^2 A$ with a factor $-10^3 V_u/(4\pi e^2 a^2) = -83$ [meV/eV^2].
34. J. W. Loram, J. Luo, J. R. Cooper, W. Y. Liang, J. L. Tallon, *J. Phys. Chem. Solids* **62**, 59 (2001).

35. Supported by the Netherlands Foundation for Fundamental Research on Matter with financial aid from the Nederlandse Organisatie voor Wetenschappelijk Onderzoek. We thank J. E. Hirsch, D. Basov, P. W. Anderson, A. J. Leggett, D. I. Khomskii, J. Orenstein, and Z. X. Shen for stimulating comments during the preparation of this work.

17 January 2002; accepted 2[illegible] February 2002

Santander-Sy

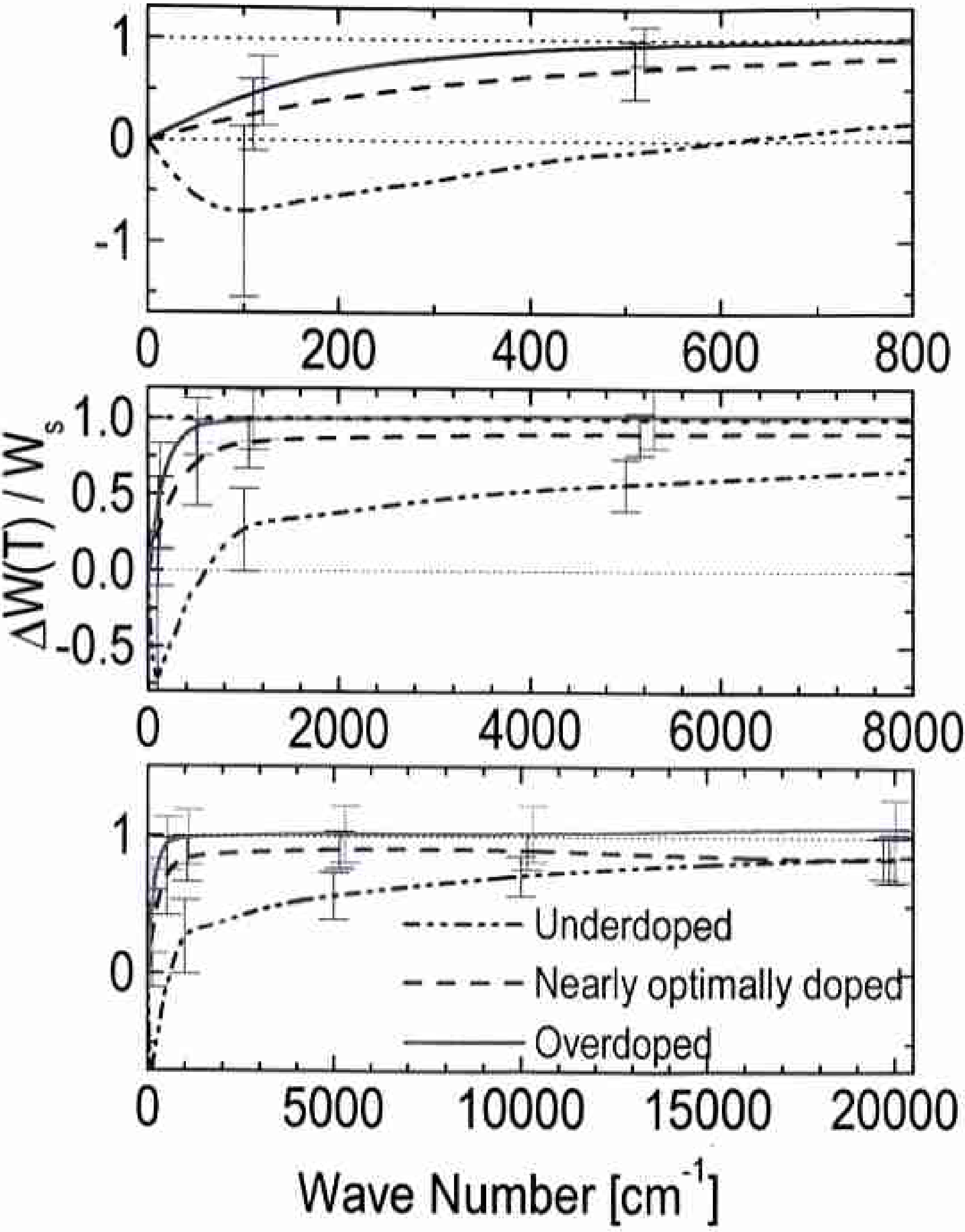

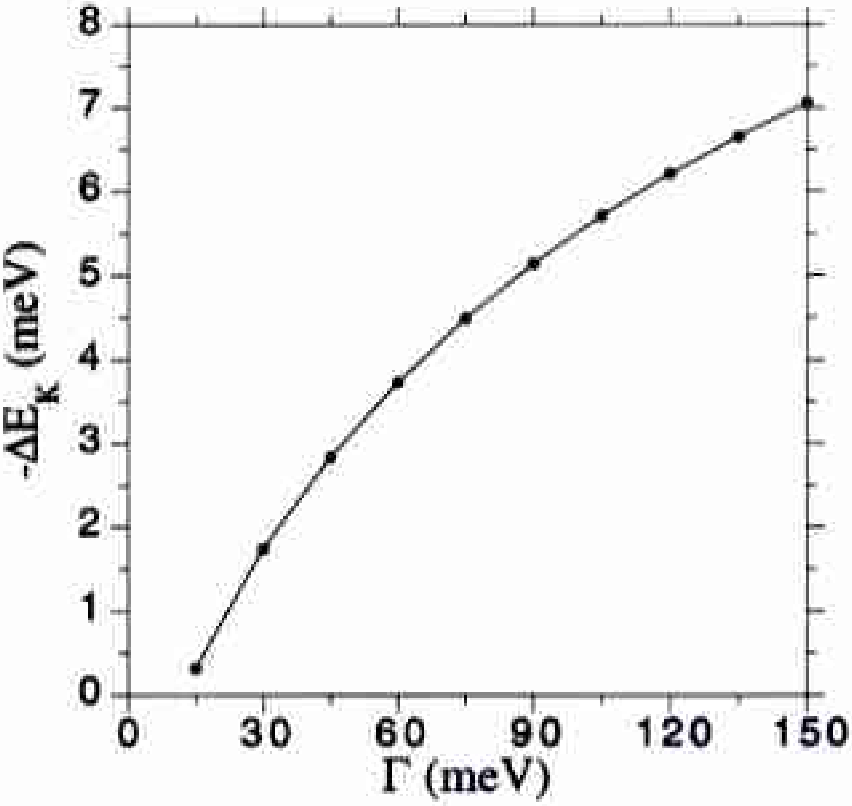
-ΔE_K (meV)
0
1
2
3
4
5
6
7
8
0
30
60
90
120
150
Γ (meV)

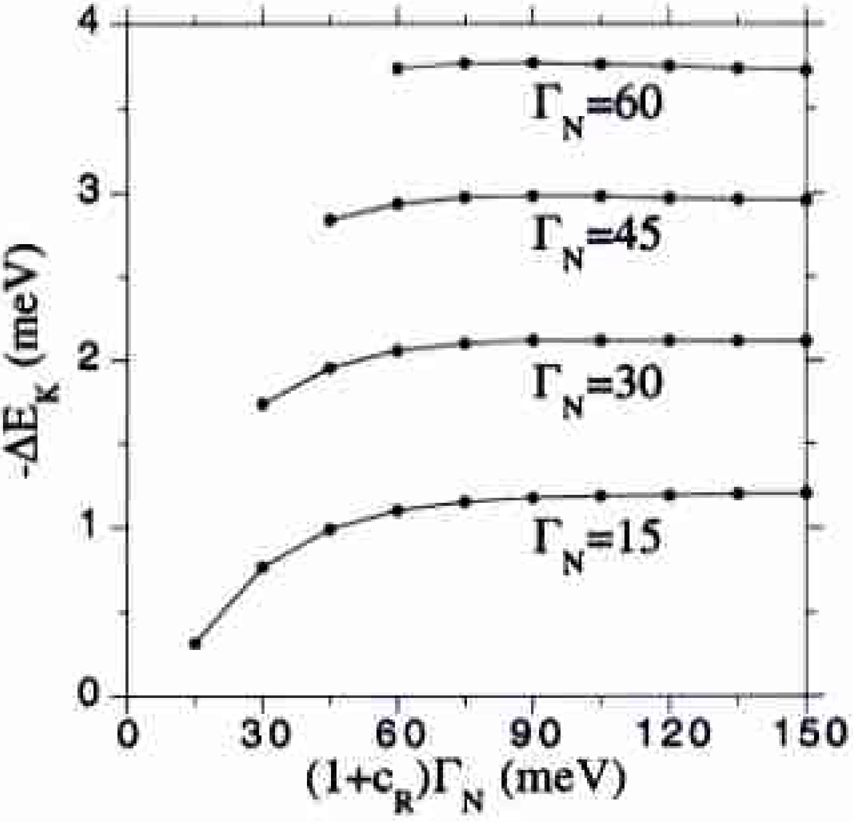
-ΔE_K (meV)
0
1
2
3
4
Γ_N=60
Γ_N=45
Γ_N=30
Γ_N=15
0
30
60
90
120
150
(1+c_R)Γ_N (meV)

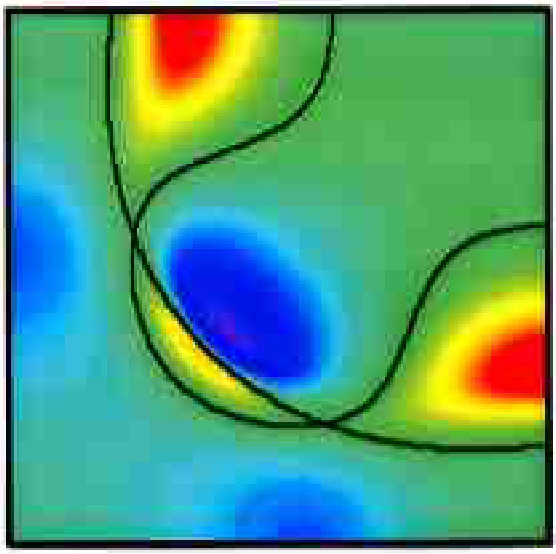

$(\nabla^2 \epsilon_k) n_k$

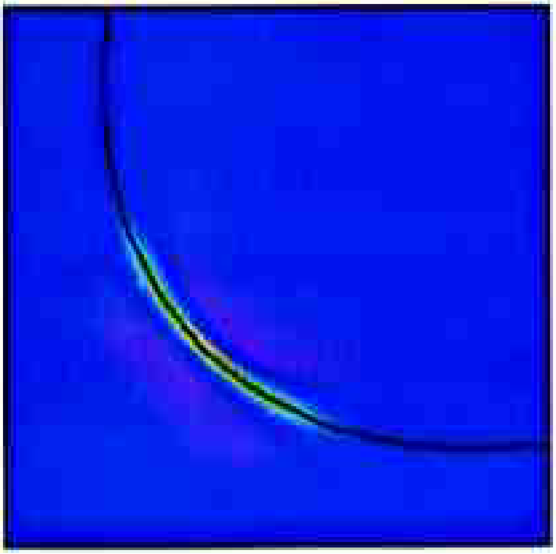

$\nabla \epsilon_k \cdot \nabla n_k$

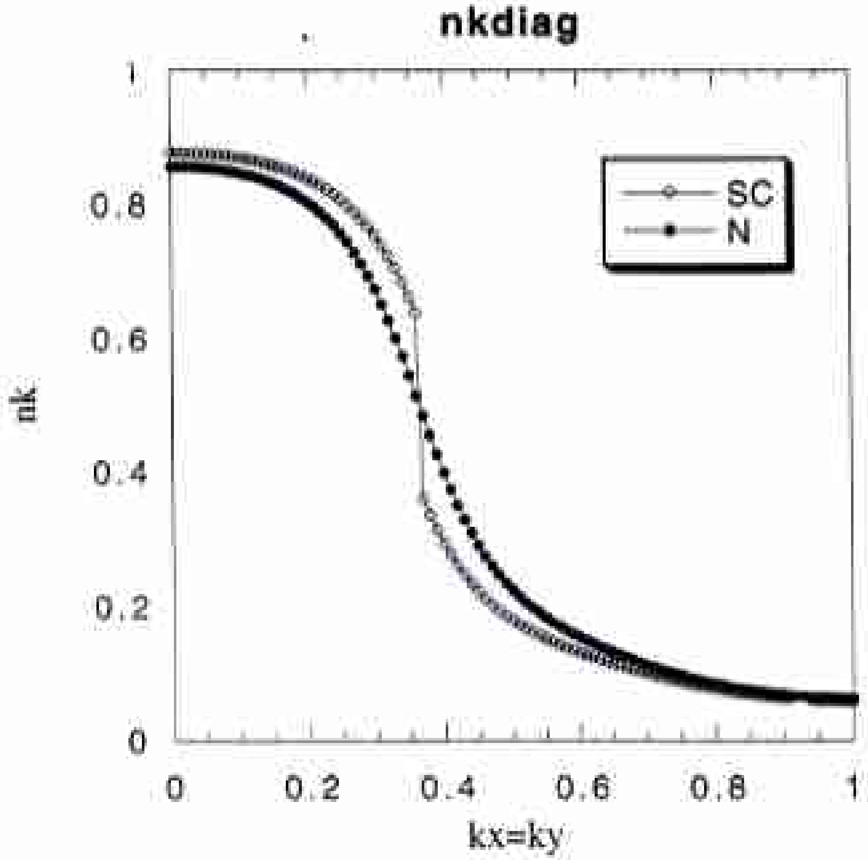
nkdiag
nk
kx=ky
SC
N
0
0.2
0.4
0.6
0.8
1
0
0.2
0.4
0.6
0.8
1

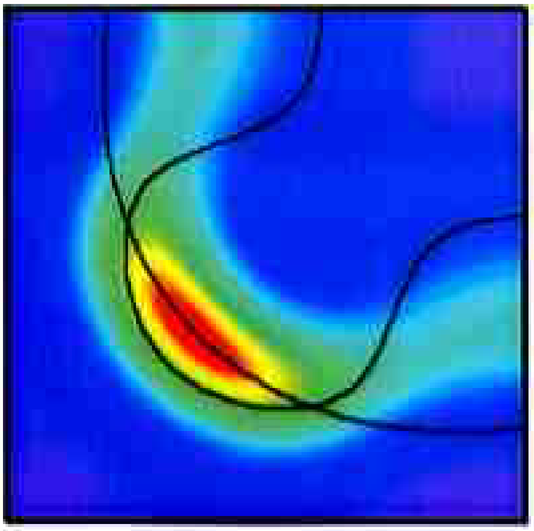

normal

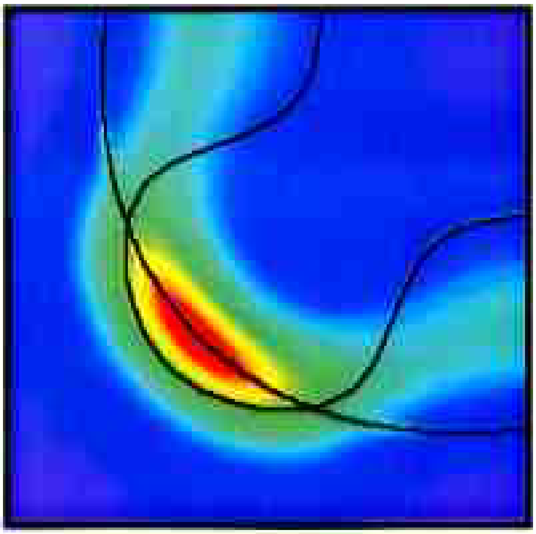

pseudogap

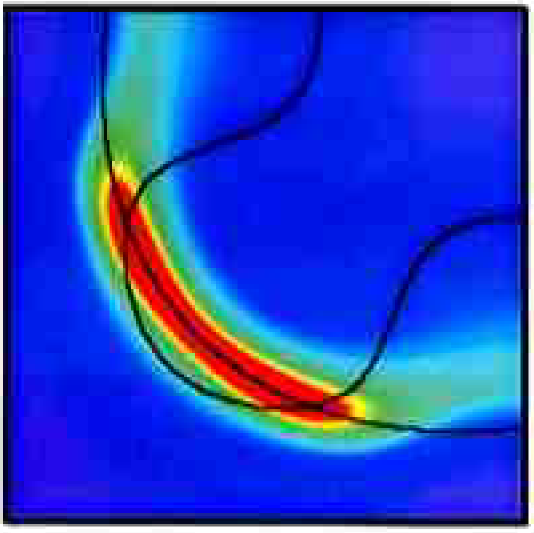

superconducting

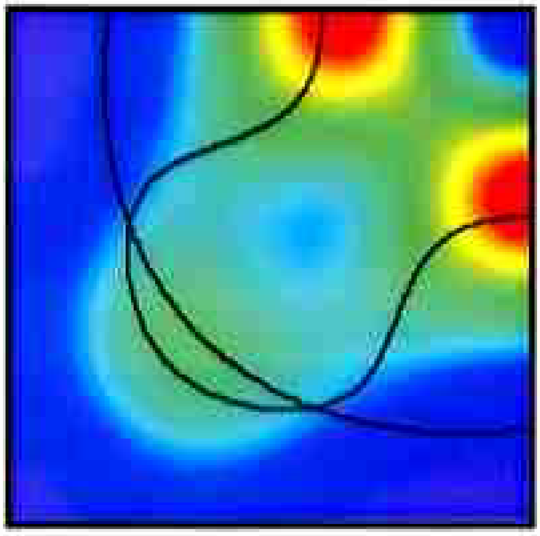

velocity

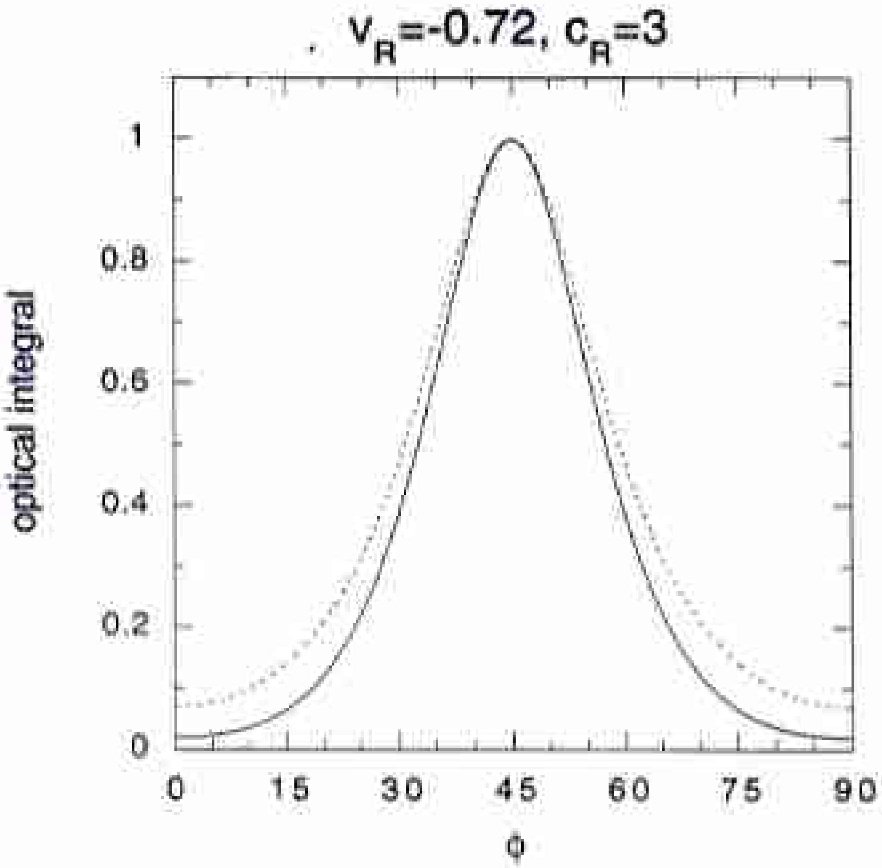
v_R=-0.72, c_R=3
optical integral
1
0.8
0.6
0.4
0.2
0
0
15
30
45
60
75
90
ϕ

PRB May

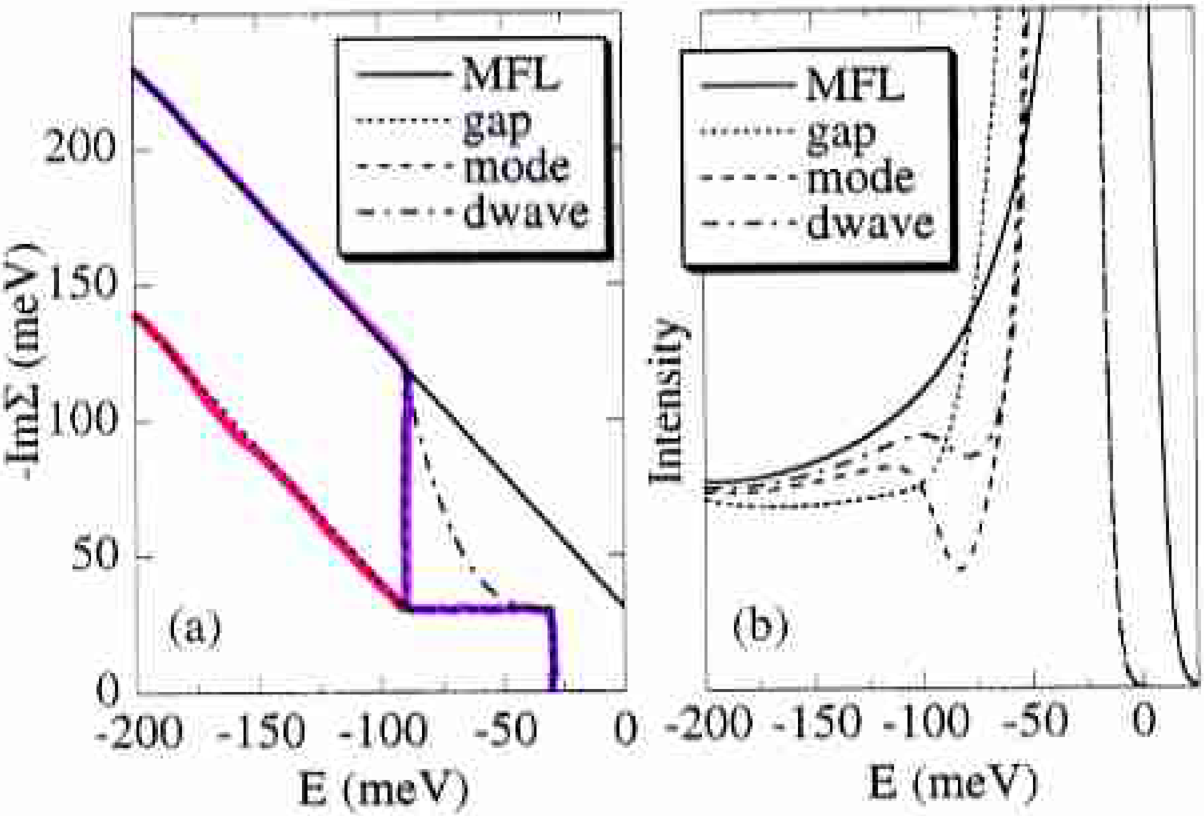

-ImΣ (meV)
200
150
100
50
0
-200
-150
-100
-50
0
E (meV)
MFL
gap
mode
dwave
(a)
Intensity
-200
-150
-100
-50
0
E (meV)
MFL
gap
mode
dwave
(b)

PRL Feb 00

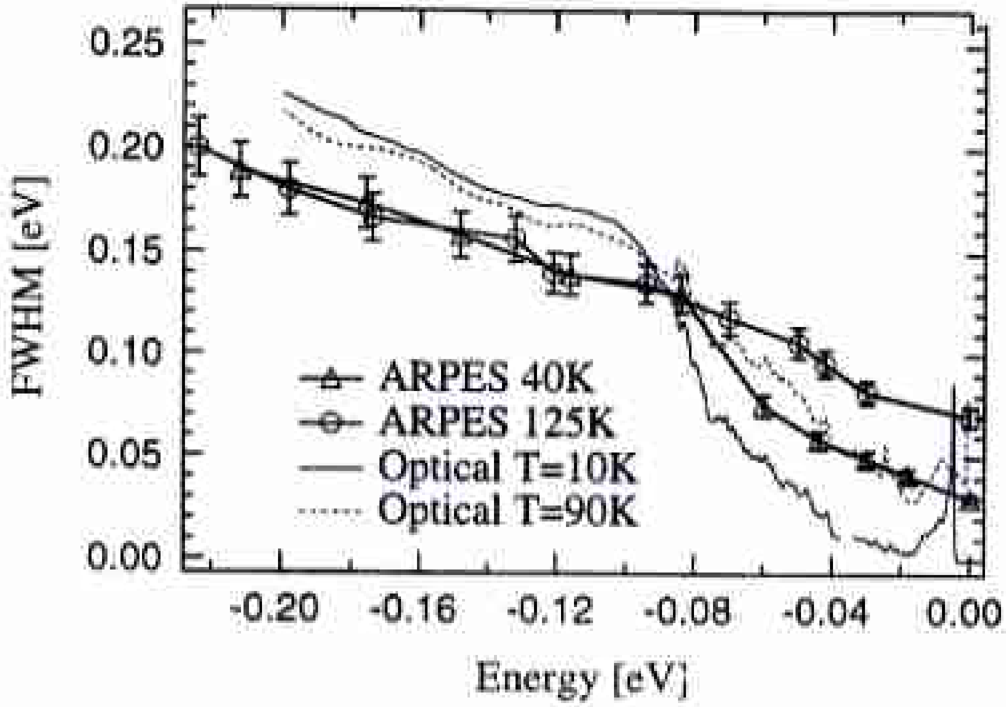

$a_k + b\omega$

PRL , Feb

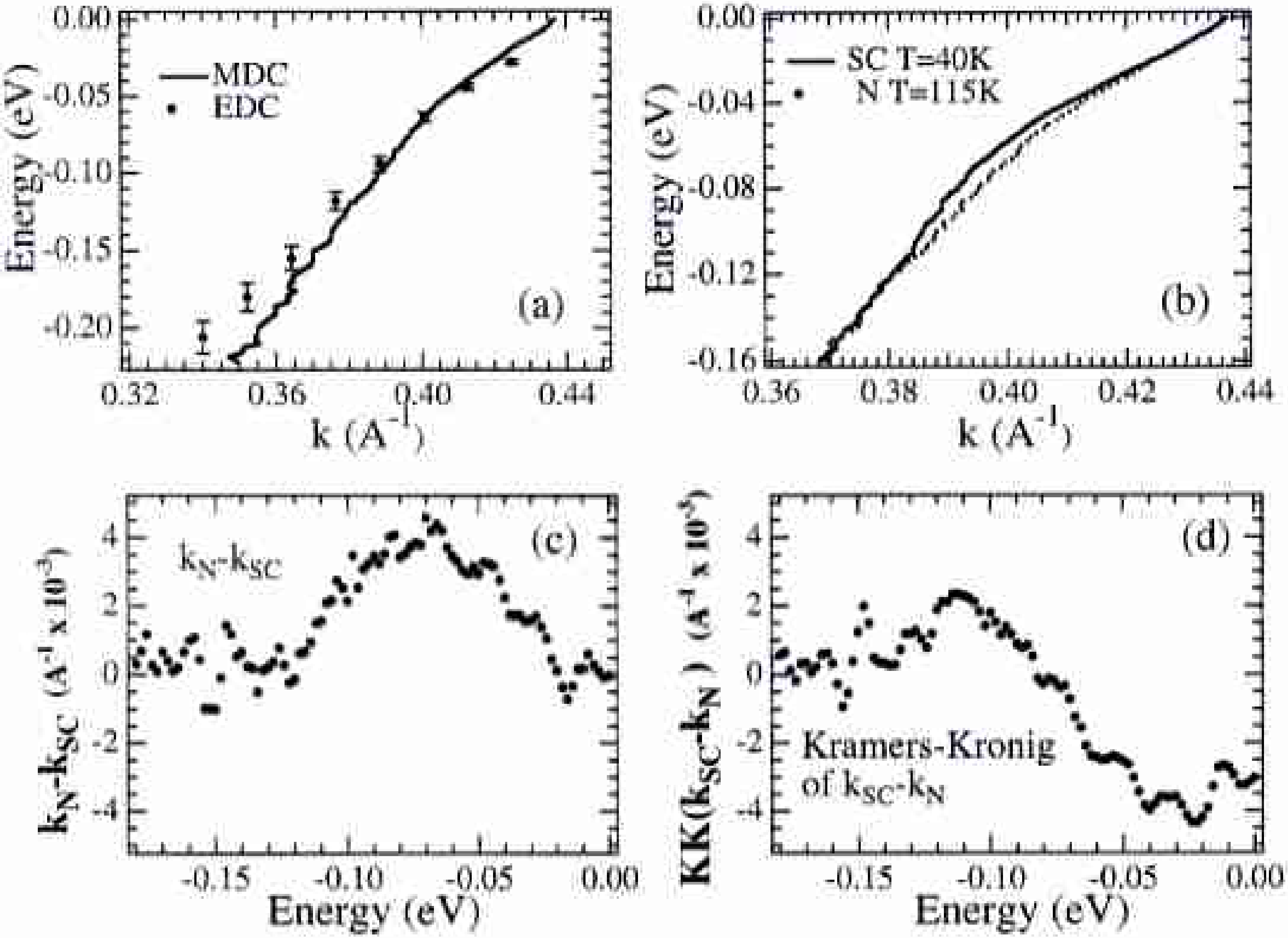

(a)
MDC
EDC
Energy (eV)
0.00
-0.05
-0.10
-0.15
-0.20
k (A^{-1})
0.32
0.36
0.40
0.44
(b)
SC T=40K
N T=115K
Energy (eV)
0.00
-0.04
-0.08
-0.12
-0.16
k (A^{-1})
0.36
0.38
0.40
0.42
0.44
(c)
k_N-k_{SC}
k_N-k_{SC} (A^{-1} x 10^{-3})
4
2
0
-2
-4
Energy (eV)
-0.15
-0.10
-0.05
0.00
(d)
Kramers-Kronig of k_{SC}-k_N
KK(k_{SC}-k_N) (A^{-1} x 10^{-3})
4
2
0
-2
-4
Energy (eV)
-0.15
-0.10
-0.05
0.00

PRL, Feb o

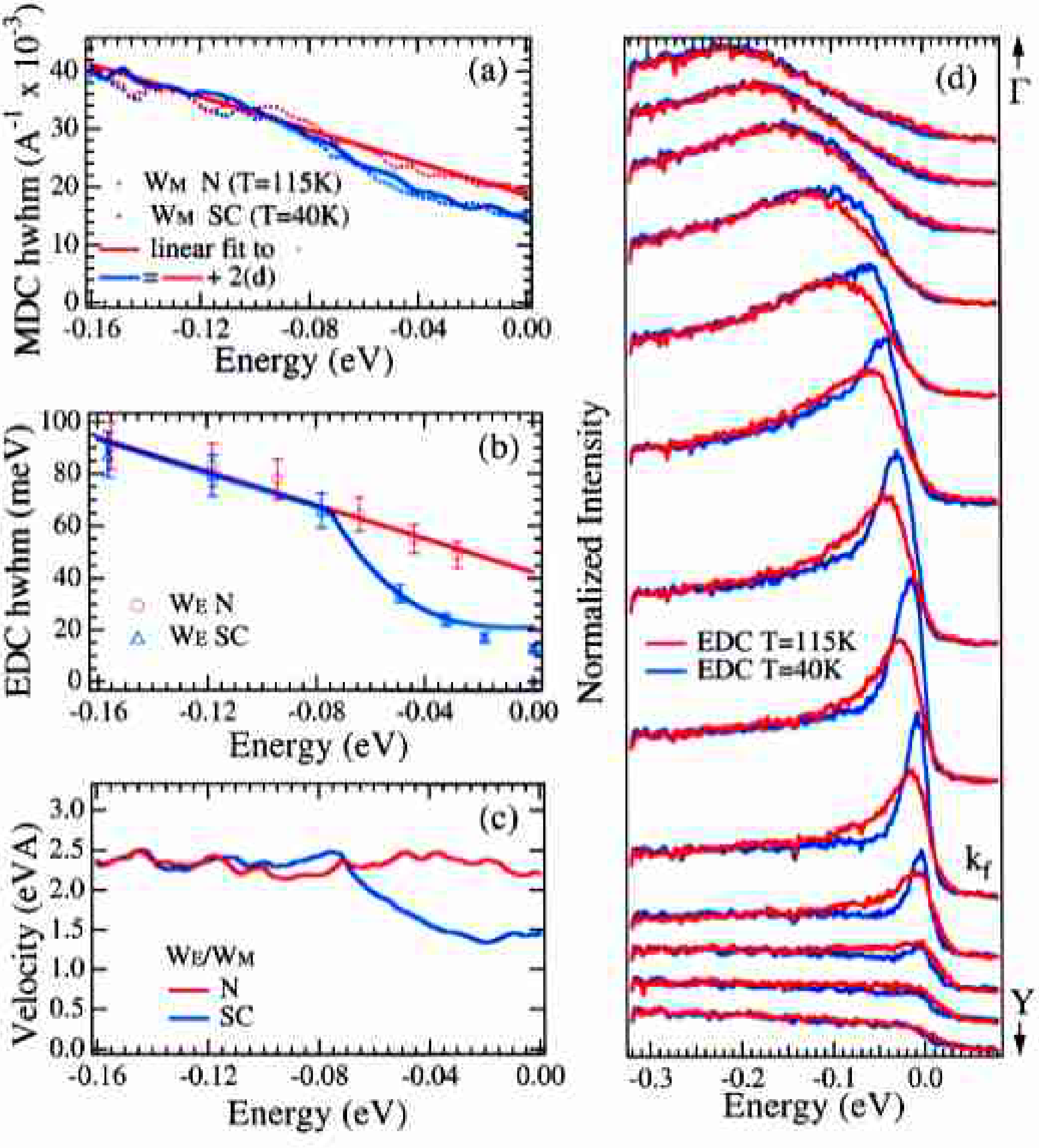
(a)
MDC hwhm (A^{-1} x 10^{-3})
40
30
20
10
0
WM N (T=115K)
WM SC (T=40K)
linear fit to
= + 2(d)
-0.16
-0.12
-0.08
-0.04
0.00
Energy (eV)
(b)
EDC hwhm (meV)
100
80
60
40
20
0
WE N
WE SC
-0.16
-0.12
-0.08
-0.04
0.00
Energy (eV)
(c)
Velocity (eVA)
3.0
2.5
2.0
1.5
1.0
0.5
0.0
WE/WM
N
SC
-0.16
-0.12
-0.08
-0.04
0.00
Energy (eV)
(d)
Γ
Normalized Intensity
EDC T=115K
EDC T=40K
k_f
Y
-0.3
-0.2
-0.1
0.0
Energy (eV)

Dispersion in momentum cuts from near node (bottom) to (π,0) point (top). Left panel is $T > T_c$, other panels $T < T_c$

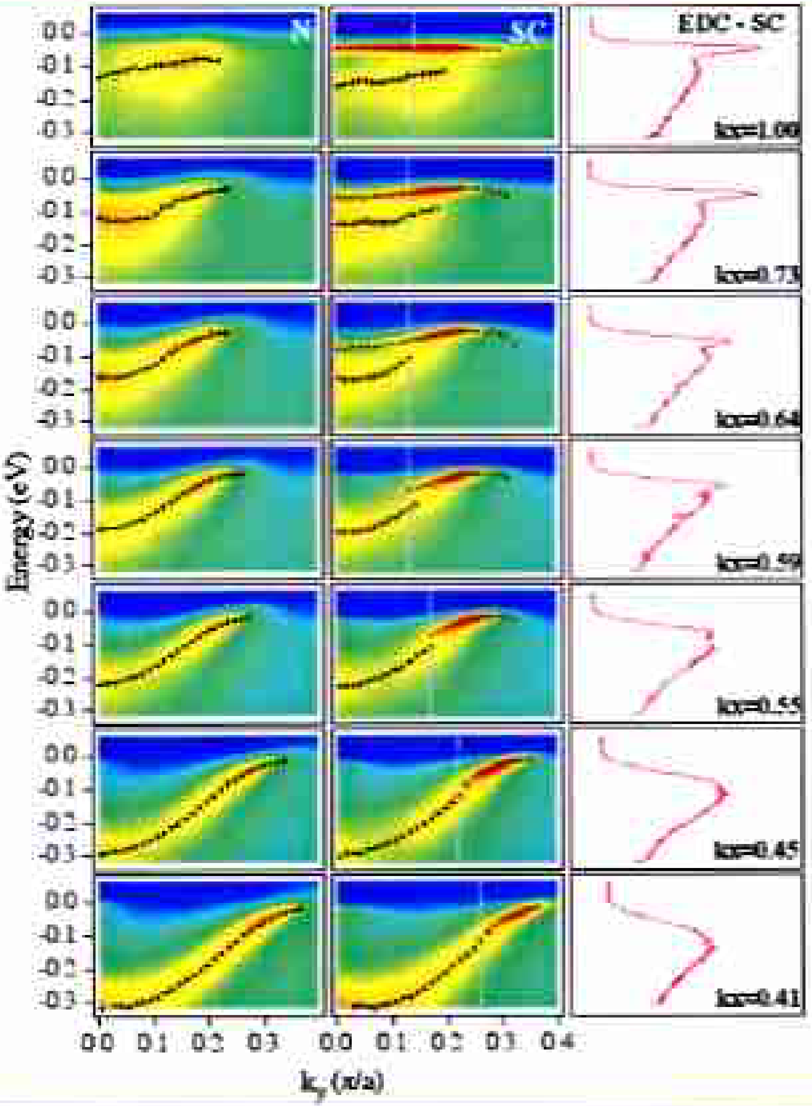

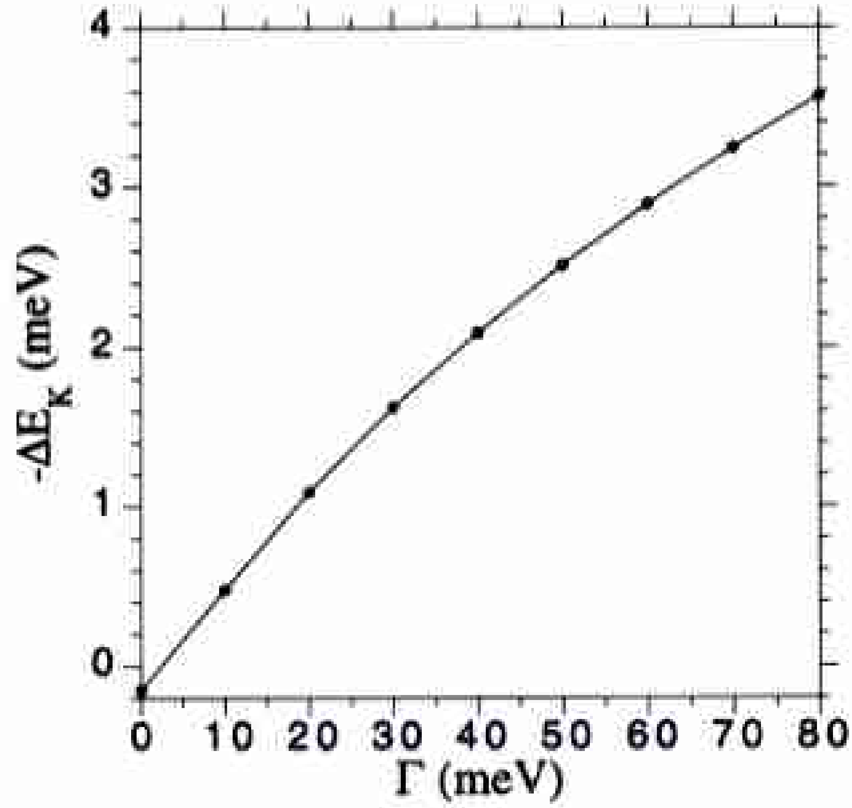

4
3
2
1
0
-ΔE$_K$ (meV)
0
10
20
30
40
50
60
70
80
Γ (meV)

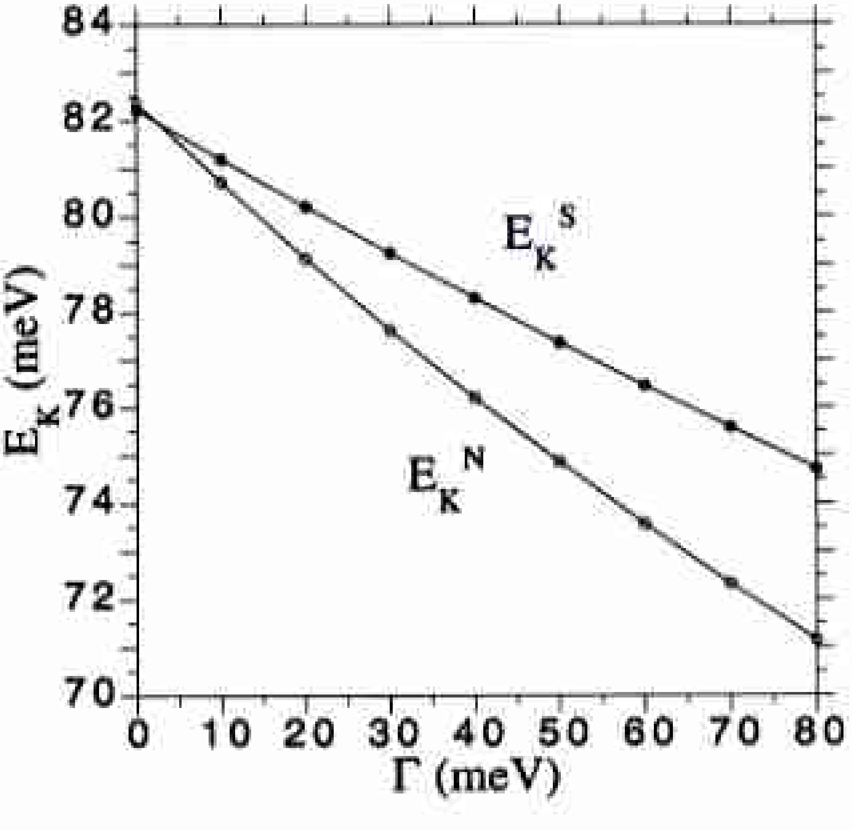

84
82
80
78
76
74
72
70
E$_K$ (meV)
E$_K$^{S}
E$_K$^{N}
0
10
20
30
40
50
60
70
80
Γ (meV)

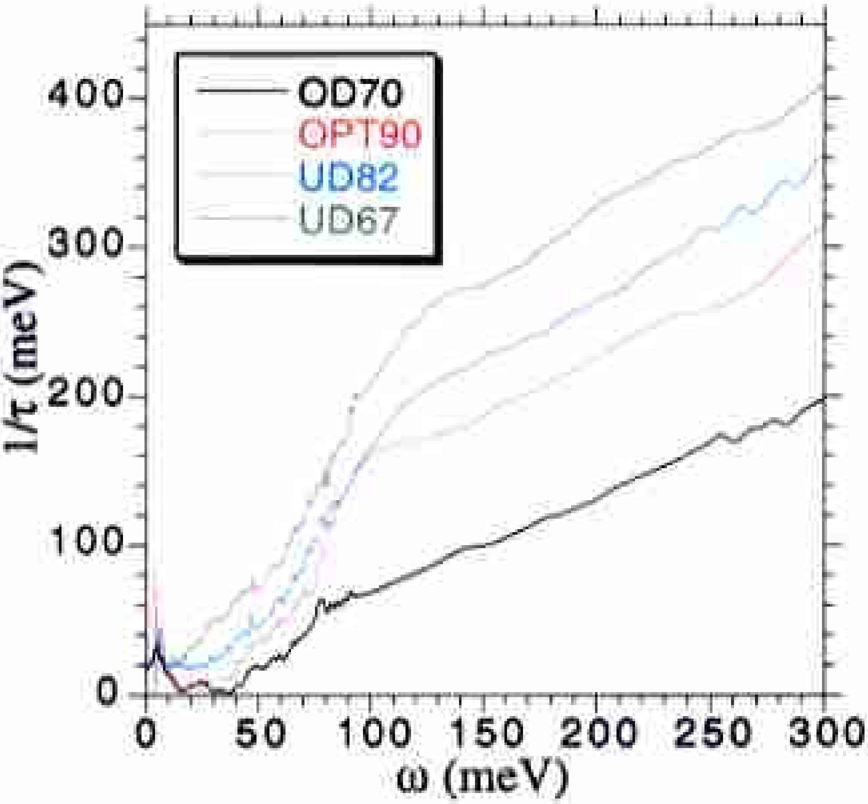
OD70
OPT90
UD82
UD67
1/τ (meV)
0
100
200
300
400
ω (meV)
0
50
100
150
200
250
300

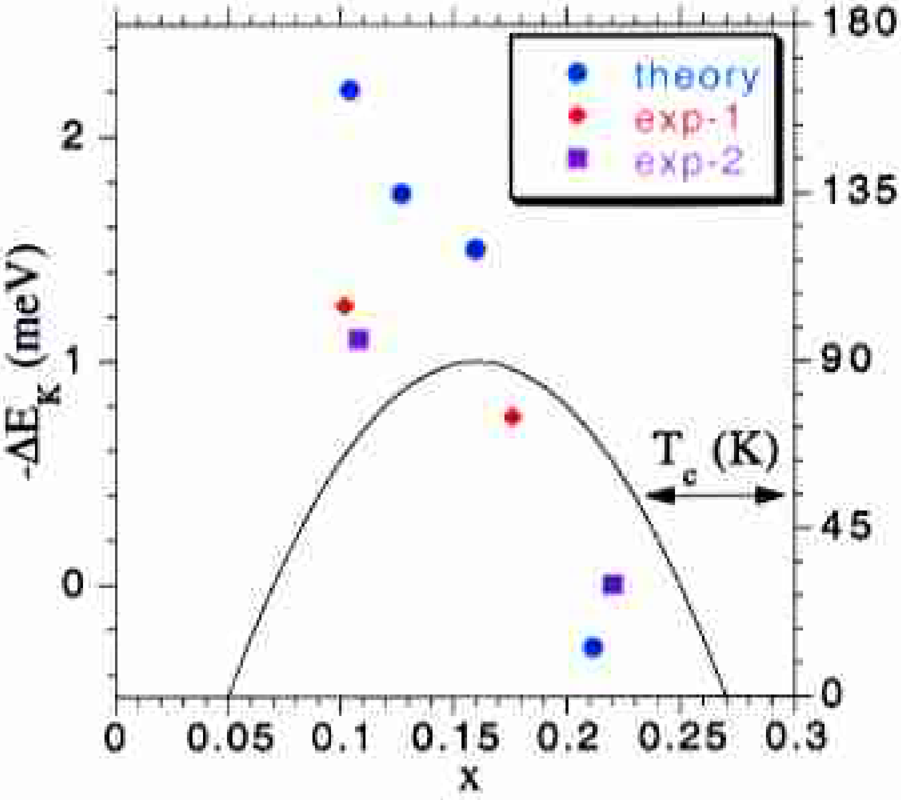
theory
exp-1
exp-2
-ΔE_K (meV)
0
1
2
T_c (K)
0
45
90
135
180
x
0
0.05
0.1
0.15
0.2
0.25
0.3